Charles University

Faculty of Sciences

Programme of study: Geology

Dissertation thesis

Ondřej Krýza

Analogue and numerical simulations of the geodynamical systems - insights from the models of the Earth collision tectonics and Martian mudflows

Analogové a numerické simulace geodynamických systémů - poznatky z modelů kolizní tektoniky na Zemi a bahenních proudů na Marsu

Institute of Petrology & Structural Geology

Supervisor: doc. Mgr. Ondrej Lexa, Ph.D.
Consultant: Mgr. Prokop Závada, Ph.D

Prague, 2020

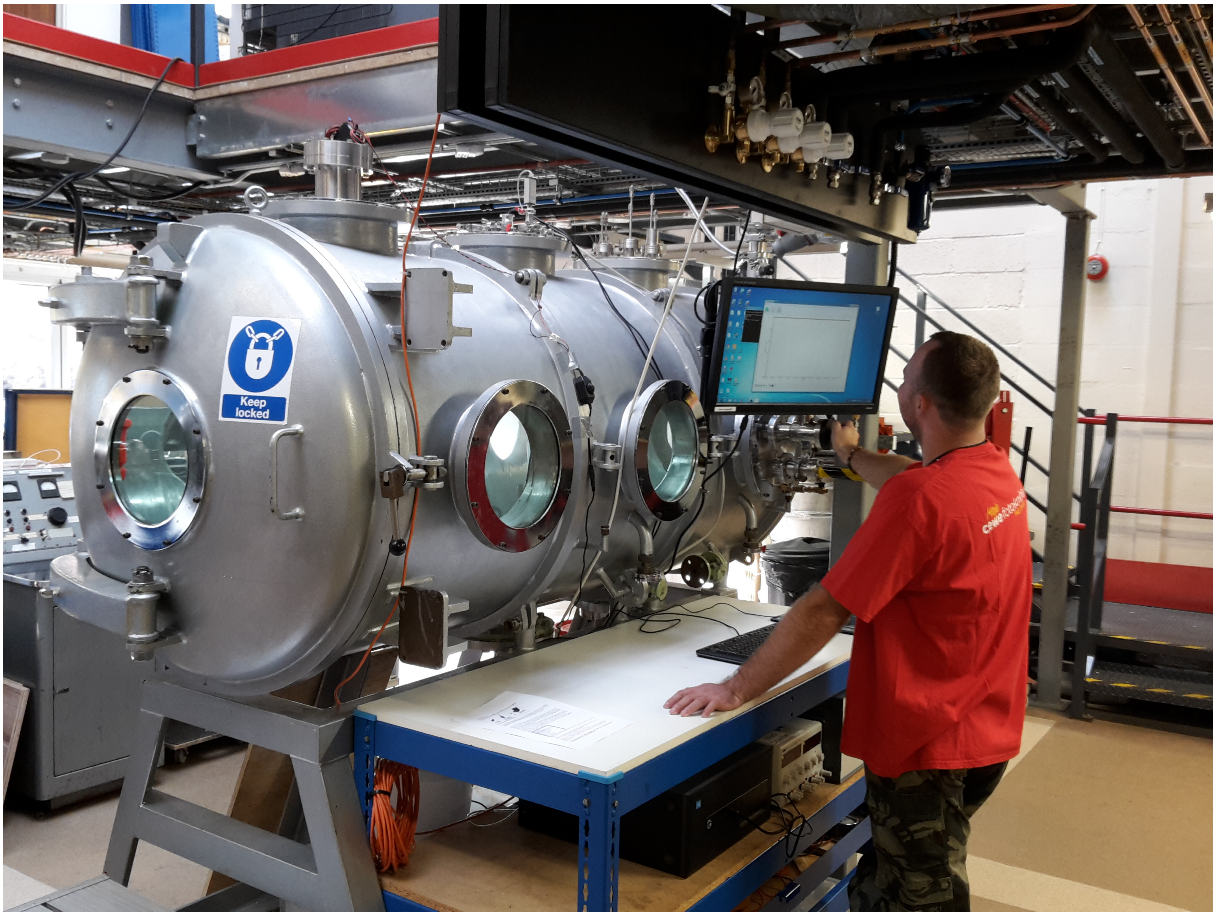

Large Mars Vacuum Chamber in the Hypervelocity Impact Facility at the Open University in Milton Keynes

This thesis represents an effort of many people that were involved to individual research projects as well as a people that contributed by discussions, technical help and moral support.
At the first place I would like to thank to my supervisor Ondrej Lexa who led me during my studies and who was always open to new ideas and discussion. Many thanks belong to Prokop Závada for all the help with the manuscripts and for fruitful cooperation on many interesting topics related to analogue modelling. Great thanks to Karel Schulmann for many interesting talks about oroclinal buckling and for help with related manuscript.
During the studies I was invited to participate on many interesting topics mainly related to modelling in geosciences and planetology. In this place I would like to thank to Petr Brož who showed me a beauties of the Mars research. Likewise, I would like to thank to Petra Maierová who consecrate me to the numerical model of the Bohemian Massif evolution and helped me with the model used in Chapter IV. Big thanks to Václav Špilar and Steve Collett for careful reading, commenting and grammar corrections of this thesis.
Also many thanks belongs to all remaining co-authors which participated on individual manuscripts and who are not mentioned namely here. As well, I appreciate all the work of the reviewers and editors and I would like to thank them for many relevant comments and ideas associated with the first versions of manuscripts.
It should be noted that significant part of this thesis would not be realized without work in the analogue modelling laboratories (at the Géosciences Rennes - University of Rennes 1, Geophysical Institute of Czech Academy of Sciences and at the Open University in Milton Keynes). This thesis was also realized with significant support from research grant projects (GAČR: 19-27682X, GAČR: 17-17540S, 16-17457S, UNCE/SCI/006, EPN2020-RI: 654208).
I am glad that I found so warm atmosphere and many good friends at both institutions where I spent the best years of my life. Thanks to my friends and colleagues from the Institute of Petrology and Structure Geology and from the Geophysical Institute of the CAS. Especially, I would like to gratefully thank to Drahomíra Seemannová for all the support and help with administrative background.
Hana Smejkalová and Sabina Sládková deserve great appreciation for huge portion of patience during all the years of my studies.
Last but not least is my family that I would like to warmly thank. This thesis will be dedicated to them.

Prohlašuji, že jsem závěrečnou práci vypracoval samostatně, a že jsem uvedl všechny použité informační zdroje a literaturu. Tato práce ani její podstatná část nebyla předložena k získání jiného nebo obdobného druhu vysokoškolské kvalifikace. Výsledky teze jsou produktem mé vlastní práce nebo práce ve výzkumném týmu.

V Praze dne 17.1. 2020 ....

I declare that this thesis is a result of my own work and that I have cited all the resources and literature. Neither this thesis nor its substantial part has been submitted to fulfill requirements for any other academic degree. The results of the thesis are my own work or the product of collaboration with other members of the research teams.

In Prague, 17.1. 2020 ....

Abstract

Analogue and numerical modelling in geosciences is an excellent tool for studying complex spatio-temporal relationships in mass and energy transfer. Recent developments and advances in plate tectonics and planetology require a combination of both approaches to simulate processes that cannot be studied directly in-situ. Advanced physical models are complemented by deformation analysis which is based on image velocimetry and photogrammetry, while numerical simulations utilize both modern and traditional methods to solve corresponding equations in complex domains.

This work compiles several models that are focused on deformation analysis associated with material and heat transfer in large accretionary systems. The second subject of the thesis represent the investigation of the formation and propagation of large mudflows in martian atmospheric conditions.

In the first part of the work we present a general overview of the problems of analogue and numerical modelling including scaling theory, governing equations, individual methods and history. In the second part of the thesis we deal with laboratory and numerical simulations of collision-indentation tectonics associated with the emergence of large accretionary systems on Earth. The last part of the thesis is devoted to experiments designed for the study of the formation and development of mudflows, which arise as a result of supposed cryovolcanic activity on the surface of Mars.

The first models involves oroclinal buckling of an accretionary belt and continental ribbon in the post-subduction stage related to the indentation of a cratonic system at an orthogonal direction. The results of the individual experiments showed a complex flow of the material of the lower crust and the upper mantle in the axial plane of both progressively buckled interlimb areas. This ductile flow is associated with the deformation response of the upper crust and with the emergence of large pop-up and pop-down domains, local faults and shear zones. The correlation of the results from the surface deformation analysis and from the deformation analysis of the orthogonal sections of the model confirms the significant exhumation of the continental and oceanic mantle in the proximal hinge area. This exhumation is correlated with the existence of a significant gravimetric anomaly in the Hangai region of the Tuva-Mongol orocline which is located within the CAOB (Central Asian Orogenic Belt).

The second series of experiments is focused on the study of the melt amount and migration style effect on the dynamics of detachment folding in the pre-indentative part of crustal domain. This thermally dependent model produces a series of folds over a thin layer of the melt that migrates along the shortening direction and is simultaneously sucked into the inter-limb zones of the resulting fold-dome structures. A method for quantifying the divergence of the PIV based velocity field in the target sub-regions of the model domain was developed to balance the inflow and outflow of this material. The correlation of the time evolution of the divergence and the amount of the melt in the individual folds internal structures revealed the polyphase

development of each fold. The systematic change in the height of the folds and the modal melt content of the individual locked folds is proportional to the rate of inflow of the melt into their cores. Overpressure of the melt in locked folds leads to its extrusion back into the source layer, where it can be further transferred along the shortening direction and support further detachment folding.

Since these models are produced in an unscaled gravitational field, potential diapiric exhumation of the lower crust is also the subject of discussion. The model of the Rayleigh-Taylor instability was used with tested variation of rheological, geometric and thermal properties. The model simulates the evolution of a large-scale lithosphere segment, related to late orogeny which is characterized by a massively thickened crustal domain, during the post-collision stage. Analysis of the selected simulations showed that the crustal-scale diapirism is typical for collisional and post-collisonal systems, that are characterized by a distinctly weak and hot lower felsic crust with developed density perturbations at the border with the overlying mafic crust. The rate of diapiric exhumation depends on the convergence rate of the indenter as well as on the amplitude/wavelength of the density perturbation and specially on the density contrast of the crustal material. The rheological parameters are controlled by time-variations of the heat redistribution from the mantle into the crust and by thermal productivity of the felsic lower crust. Diapirism and folding are involved in dependence on the slowing of the convergence and on distance of the perturbation from the indenter.

The last part of the thesis presents physical modeling of the mudflows propagating in atmospheric conditions at the surface of Mars. The series of more than sixty experiments was designed to study mudflow on both cold and hot surfaces made of granular unconsolidated material (sand) or solid consolidated material (plastic plate). The effect of the subsoil inclination on the distribution and shape of mudflows was also tested.

Experiments, conducted on pre-cooled sand, revealed significant geomorphological similarity between mudflows produced at reduced atmospheric pressure and Pahoehoe lava flows at the Earth's surface atmospheric pressure. The emergence of mudflows reflects several development stages, including initial surface flow, mud degassing / freezing, and flow in closed channels with a progressive propagation at the head of the stream. The mud propagation through an enclosed channel and progressive development of the lobes in the stream foreland is similar to the development of pillow lavas on Earth.

Experiments conducted on a warm sand substrate revealed a different process of transporting mud material that combines 'classical flows' and 'levitation' of mud above a warm surface, depending on the distance from the source area.

Keywords

Analogue modelling, Numerical modelling, Orocline, Detachment folding, PIV analysis, DEM models, Diapirism, Mudflows, Mars

Abstrakt

Analogové a numerické modelování v geovědách představuje vynikající nástroj ke studiu složitých časoprostorových vztahů při transferu hmoty a energie. Současný rozvoj a pokrok na poli deskové tektoniky a planetologie vyžaduje kombinaci obou přístupů pro simulaci procesů, které nelze studovat přímo in situ. Pokročilé fyzické modely jsou doplňovány deformační analýzou vycházející z obrazové velocimetrie a fotogrammetrie zatímco numerické simulace využívají moderních i tradičních metod pro řešení příslušných rovnic ve složitých doménách.

Předkládaná práce kompletuje několik typů modelů, které jsou zaměřeny jednak na deformační analýzu spojenou s transferem materiálu a tepla v akrečních systémech, tak i na simulaci vzniku a vývoje rozsáhlých bahenních proudů v atmosférických podmínkách Marsu.

V první části práce uvádíme obecný přehled problematiky analogového a numerického modelování včetně škálovacích vztahů, řídících rovnic, jednotlivých metod a historie. Ve druhé části práce se zabýváme laboratorními i numerickými simulacemi kolizní-indentační tektoniky spojené se vznikem velkých akrečních systémů na Zemi. Poslední část práce je věnována experimentům navrženým pro studium vzniku a vývoje bahenních proudů, které vznikají v důsledku předpokládané kryovulkanické činnosti na povrchu Marsu.

První série modelů zahrnuje oroklinální ohyb akrečního pásu a kontinentálního žebra v post-subdukční etapě, který je způsobený indentací kratonického systému v ortogonálním směru. Výsledky experimentů prokázaly komplexní tok materiálu spodní kůry a svrchního pláště v osní rovině obou vznikajících zámkových oblastí, který je spojen s deformační odezvou svrchní kůry a vznikem rozsáhlých násunovo-poklesových domén i střižných zón. Kinematika, dynamika a geometrie těchto svrchno-korových deformačních struktur byla analyzována pomocí fotogrammetrických metod (DEM) a obrazové rychlostní analýzy (PIV). Korelace povrchové deformační analýzy a deformační analýzy ortogonálních řezů modelu potvrzuje významnou exhumaci kontinentálního i oceánského pláště v proximální zámkové oblasti. Tento efekt je korelován s existencí významné gravimetrické anomálie v Hangaiském regionu Tuva-Mongolské orokliny situované v rámci CAOB (Central Asian Orogenic Belt).

Druhá série experimentů je zaměřena na studium vlivu migrace a množství taveniny na dynamiku vrás odlepení v před-indentační korové doméně. Tento termálně závislý model produkuje sérii vrás nad tenkou vrstvou taveniny, která migruje podél směru zkracování a je souběžně nasávána do meziramenních zón vznikajících vrásovo-dómových struktur. Pro bilanci vtoku a výtoku tohoto materiálu byla vyvinuta metoda využívající kvantifikaci divergence rychlostního pole produkovaného PIV analýzou v cílových podoblastech modelové domény. Korelace časové změny divergence a množství taveniny v jednotlivých vrásách odhalila polyfázový vývoj každé vrásy. Systematická změna ve výšce vrás a modálním obsahu taveniny v jednotlivých uzamčených vrásách je úměrná rychlosti vtoku taveniny do jejich jader. Přetlakování taveniny v uzamčených vrásách vede k jejímu vytlačení zpět do zdrojové vrstvy, kde může být dále přenesena ve směru zkracování a usnadnit tak další odlepené vrásnění.

Neboť tyto modely jsou produkovány v neškálovaném gravitačním poli, byla rovněž diskutována potenciální diapirická exhumace spodnokorového materiálu. Byl použit model Rayleigh-Taylorovy nestability s variací reologických, geometrických a termálních vlastností spodní kůry pozdně orogení a ztluštěné litosférické domény. Analýza vybraných simulací ukázala, že korový diapirismus je charakteristický pro kolizní systémy, které jsou typické výrazně ‘měkkou’ a teplou spodní felzickou kůrou s výrazně vyvinutou hustotní perturbací na hranici s nadložní mafickou kůrou. Tvar diapirismu je ovlivněn viskozitním kontrastem korových vrstev a rychlostí konvergence. Rychlost diapirické exhumace závisí na rychlosti konvergence indentoru, amplitudě a vlnové délce hustotní perturbace a hustotním kontrastu materiálu spodní kůry. Reologické parametry jsou řízené časově proměnlivou distribucí tepla z pláště a tepelnou produktivitou felzické spodní kůry. Diapirismus a vrásnění se zastupují v závislosti na zpomalování konvergence a vzdálenosti od indentoru.

Poslední část práce prezentuje fyzické modelování bahenních proudů v atmosférických podmínkách Marsu. Série více než šedesáti experimentů byla navržena pro studium toku bahna po chladném i horkém povrchu tvořeném granulárním nezpevněným materiálem (písek) nebo pevném konsolidovaném materiálu (plastická deska). Rovněž byl testován vliv úklonu podloží na distribuci a tvar bahenních proudů. Všechny experimenty probíhaly při tlaku 7 mbar s různými rychlostmi extruze bahna. Pro studium topografických charakteristik jednotlivých proudů byla použita metoda rekonstrukce DEM na základě pořízených fotografií povrchu modelu.

Série experimentů probíhajících na podchlazeném písku prokázala významnou geomorfologickou podobnost mezi bahenními proudy ve sníženém atmosférickém tlaku a lávovými proudy typu Pahoehoe v pozemském povrchovém tlaku. Vznik bahenního proudu reflektuje několik vývojových stádií, které zahrnují počáteční povrchový tok, odplyňování/mrznutí bahna a tok v uzavřených kanálech s progresivní propagací v čele proudu. Proces propagace z uzavřeného kanálu je podobný výlevům polštářových bazických láv na Zemi.

Experimenty probíhající na teplém pískovém podkladu odhalily odlišný proces transportu bahenního materiálu, který kombinuje ‘klasický proud’ a ‘levitaci’ bahna nad teplým povrchem v závislosti na vzdálenosti od zdrojové oblasti.

Klíčová slova

Analogové modelování, numerické modelování, oroklina, vrásy odlepení, PIV analýza, DEM modely, diapirismus, bahenní proudy, Mars

List of related papers and authors contribution

This thesis is a monography combined with one published paper, two manuscripts under review and one manuscript before submitting. The candidate is the first author on two of them and contributed as second author to two others.

Krýza, O., Závada, P., & Lexa, O. (2019). Advanced strain and mass transfer analysis in crustal-scale oroclinal buckling and detachment folding analogue models. *Tectonophysics*, **764**, 88-109.

- Article is related to Chapter 3. Candidate was responsible for all modelling, programming of all procedures, PIV and DEM calculations, data processing and analysis. Candidate prepared all figures and original text body except paragraph related to scaling of detachment folding model. The careful reading and modifications of text were made by co-authors.
  (Authors contribution: 70%)

Krýza, O., Lexa, O., Schulmann, K., Guy, A., Gapais, D., Cosgrove, J. & Xiao, W. Oroclinal buckling and associated lithospheric-scale material flow - insights from physical modelling: implication for Mongolian orocline. In prep.

- Article is related to Chapter 2. Candidate designed and conducted all models. Candidate is responsible for PIV and DEM calculations, data processing and analysis. Candidate prepared most of the figures and main text body which was improved with co-authors.

Brož, P., Krýza, O., Wilson, L., Conway, S.J., Hauber E., Mazzini A., Raack, J., Patel, M.R., Balme, M.R. & Sylvest, M.E. (2019) Lava-like mud flows on Mars. *Nature Geoscience*, In review

- Article is related to Chapter 5. Candidate contribution was co-designing of the methodology, model setup and data analysis. Candidate calculated all DEM models.
  (Authors contribution: 40%)

Brož, P., Krýza, O., Conway, S.J., Mueller, N.T., Hauber E., Mazzini A., Raack, J., Patel, M.R., Balme, M.R. & Sylvest, M.E. (2019) Mud Flow Levitation on Mars: Insights from Laboratory Simulations. *Earth and Planetary Sciences Letters*, In review

- Article is related to Chapter 6. Candidate contribution was co-designing of the methodology, model setup and data analysis. Candidate calculated all DEM models.
  (Authors contribution: 40%)

I certify that the above descriptions are accurate and representing the involvement of the candidate in the aforementioned research articles.

Signed:

Doc. Mgr. Ondrej Lexa, PhD.

Project supervisor

Contents

"Kryten, you have a real gift. You make things that are really, really complicated sound really, really complicated."

— A.J. Rimmer

Part I

Introduction to geodynamical modelling

1 Analogue and numerical simulations

1.1 Introduction

Analogue and numerical modelling represent powerful tools in many fields including the physical sciences, natural sciences, engineering and others. Both approaches represent also an increasingly well established technique in geosciences. The employment of the analogue techniques in this branch is historically older but, as well as numerical modelling, is currently used to simulate a wide range of problems.

While analogue modelling employs mainly the principles of dynamic and kinematic similarity between the laboratory experiment and real natural situations (e.g Hubbert, 1937; Ramberg, 1981; Weijermars and Schmeling, 1986; Brun, 2002; Cagnard et al., 2006; Bajolet et al., 2012; Pastor-Galán et al., 2012; Bajolet et al., 2013; Strak and Schellart, 2014; Bajolet et al., 2015; Kettermann et al., 2016; Brune et al., 2017), numerical modelling involves algorithm based solutions to a discretized equation system, which describes the dynamics of the studied system, and physical properties of the materials (e.g. Podladchikov et al., 1993; Burg and Ford, 1997; Beaumont et al., 2001; Gerya et al., 2002; Beaumont et al., 2004; Duretz et al., 2011a; Tackley, 2012; Tackley et al., 2013; Gerya et al., 2015; Menant et al., 2016)(Fig. 1). In many current studies, both approaches to modelling are even combined and mutualy compared, given that an analogue model is simplified – marked by limited geometric or physical properties, and the numerical approach is first tested against the simplified analogue model and then further developed to involve the complex geometry, rheology, or a time scale of a given geodynamic process (e.g. Buiter et al., 2016; Schreurs et al., 2016; Warsitzka et al., 2017; Menant et al., 2016; Brune et al., 2017; Zwaan and Schreurs, 2017).

The output of the numerical modelling approach is a serie of a discrete model data, either in the form of point values (pressure, temperature, density, viscosity, etc) or fields (velocity, strain(-rate), potential energy, volume changes, integral or average values of temperature, pressure, etc.).

The analysis of analogue models is generally more complex than analysis of numerical models, since it is usually not possible to obtain all of the physical parameter data at selected points of the model domain. Thus, finite model state has been historically studied in orthogonal section views or topographical views of the model surface, while the inner dynamics and structures were roughly reconstructed from only a few cross-sections and time frames. In addition, quantification of the deformation typically required manual calculations of the strain from changes of the angles and distances between the material marker lines (e.g. square grids at the model surface). However, with the development of digital imaging equipment and the growing potential of computing, nowadays, it is possible to accurately calculate the velocity and strain fields using the PIV (Particle Image Velocimetry) or DPIV (Digital Particle Image Velocimetry) methods in a documented areas of the model (e.g.

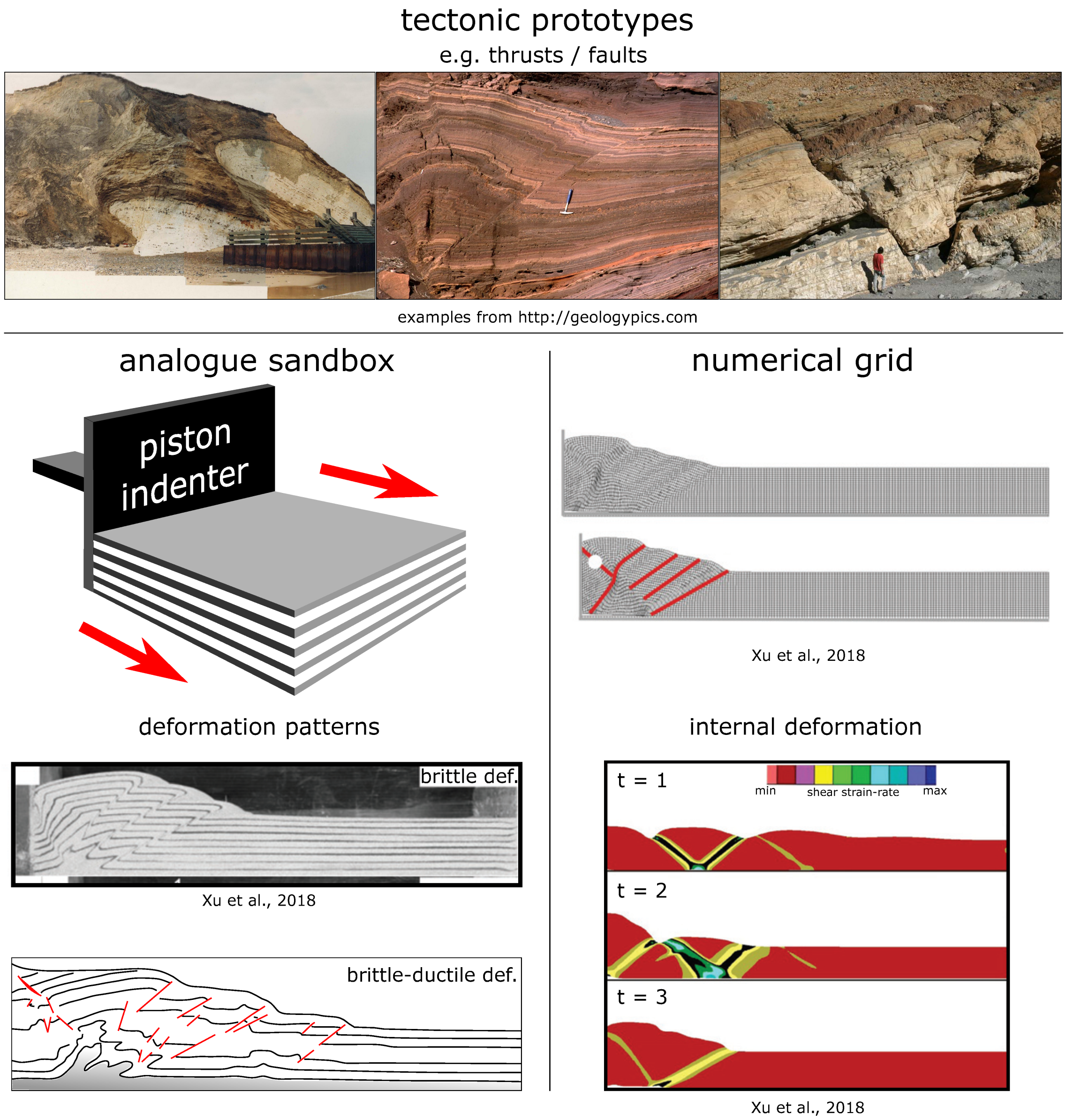

Fig. 1: Examples of analogue and numerical modelling results in geology. The model domain is prepared with respect to the natural situation (e.g. thrusting, faulting, shearing, folding etc.) and employing the analogue materials (in the case of physical models) or implemented by physical equations, coded in a computer software platform. In the analogue sandbox, the prepared model domain is progressively physically deformed while in the numerical grid domain, all deformation features are derived from the calculated velocity field according to a prescribed and discretized differential equations. Examples and comparison of both approaches are presented e.g. by Xu et al. (2018).

Strak and Schellart, 2014; Boutelier, 2016). The topography or the internal structure of the model can be also reconstructed using the photogrammetric methods (e.g. Galland et al., 2016), or X-ray tomography (e.g. Colletta et al., 1991; Pastor-Galán et al., 2012; Graveleau et al., 2012; Adam et al., 2013).

The brief introductory part summarizes the historical development of both modeling approaches, together with their philosophy, principles, applications and future potential.

1.2 Brief history and advances in analogue modelling

The history of analogue modeling is older than the numerical approach and dates back to the early 19th century. One of the first modellers in geosciences was James Hall, who was interested in fold systems (that he produced in a simple compression apparatus by compressing layers of clay), lava flows, or layered sequences and their geometric relationship with granitic bodies (Hall, 1812; Hall, 1805 and Hall 1815). These early works of James Hall are described in detail by Giorgio Ranalli (Ranalli, 2001). The studies of modelling of geological structures that followed in the rest of the century were mainly focused to the study of the fractures, faults, thrusts or folds (e.g. Favre, 1878a, Favre, 1878b, Daubre, 1879, Schardt, 1884, Cadell, 1889, Willis, 1893). Since the beginning of the 20th century, the range of problems addressed by this technique greatly expanded. and comprised the local deformation events associated with brittle and ductile tectonics and regional geodynamic processes including, for example, large-scale folding (e.g. Mead, 1920; Ramberg, 1964), thrusting and normal faulting (e.g. Hubbert, 1951), salt tectonics or formation of diapiric structures (e.g. Escher and Kuenen, 1929; Parker and McDowell, 1955; Berner et al., 1972), fracturing (e.g. Cloos, 1955), orogenesis (e.g. Kuenen, 1936), mantle flow (e.g. Griggs, 1939), boudinage and plutonism (e.g. Ramberg, 1955; Ramberg, 1970) and development of mantle plumes (e.g. Whitehead and Luther, 1975). Proto-subduction (e.g. Kuenen, 1936) has also been studied in the pre-plate tectonics era, and since the 1960s, more and more extensive regional models associated with divergent interfaces and rifting (e.g. Benes and Davy, 1996; Corti et al., 2003) have been also involved in an increasing number of studies. Another group of studies investigated the strain development during transform and transcurrent motion along discrete interfaces (e.g. Dauteuil and Mart, 1998), advanced models of convergent zones (including collision and indentation tectonics) (e.q. Tapponnier et al., 1982, Davy and Cobbold, 1988) and subduction of the lithosphere (e.q. Jacoby, 1973).

A more detailed list of the works and a review related to the analogue modelling over the past century was compiled by Schellart and Strak (2016) or Koyi (1997). Various examples of the application of analogue modelling to geodynamic problems are shown in (Fig. 2).

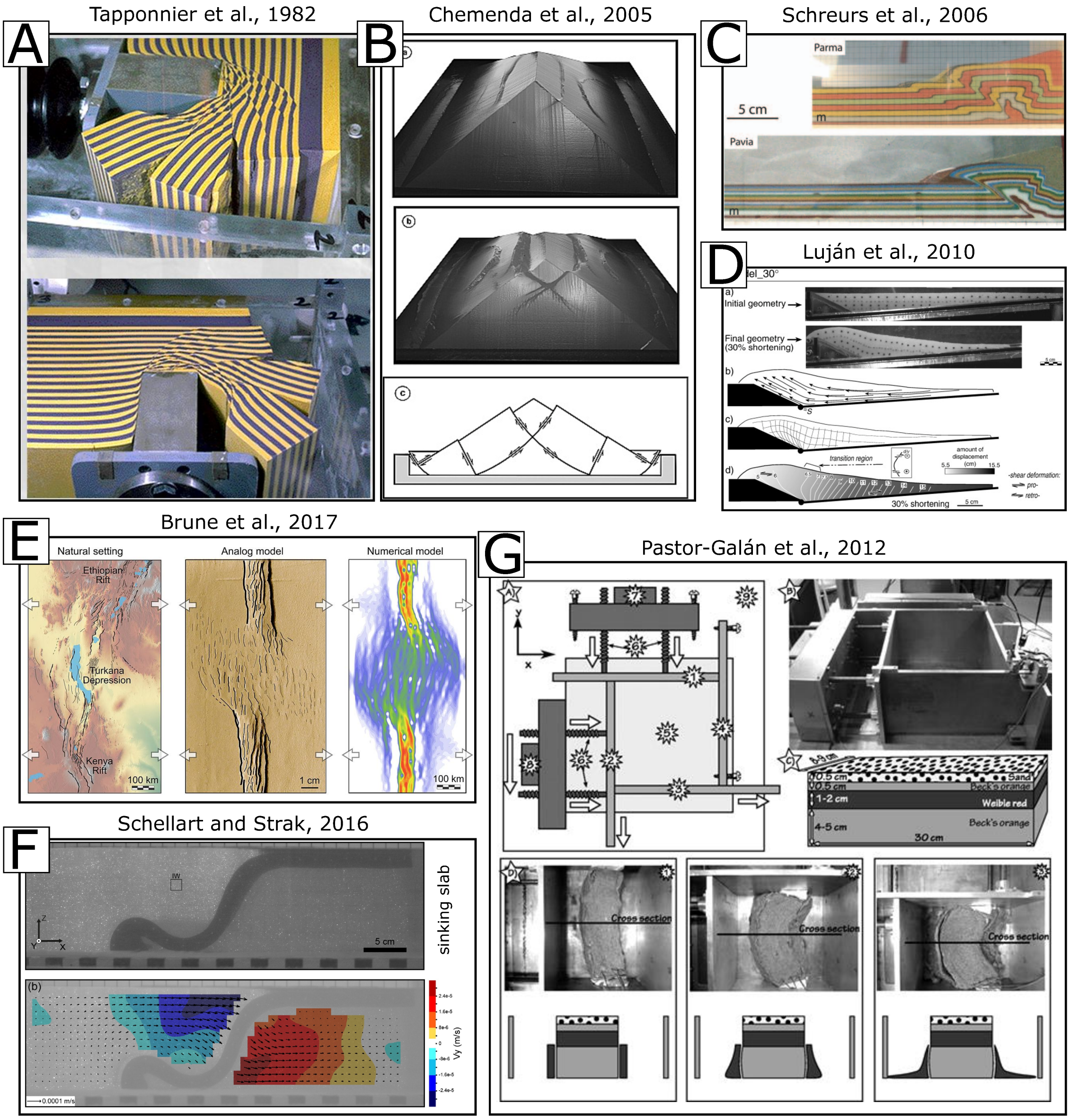

Fig. 2: Examples of analogue modelling of various geodynamical problems. From upper-left corner: (A) the indentation of the Indian plate in to the Euro-Asian plate (Tapponier et al., 1982); (B) deeply seated landslides under artificial gravitational acceleration (Chemenda et al., 2005); (C) the development of brittle thrust wedges (Schreurs et al., 2006); (D) the study of flow trajectories in viscous orogenic wedges (Luján et al., 2010); (E) centrifuge modeling of rifting in a lithosphere with inherited extension structures (Brune et al., 2017); (F) models of slab subduction and associated asthenospheric flow (Schellart and Strak, 2016) and (G) modelling of oroclinal buckling (Pastor-Galán et al., 2012).

1.3 Scaling of the analogue models

In 1937, M. K. Hubbert introduced a theory describing the principle of scaling analogue models with respect to a corresponding natural pattern - “prototype” (Hubbert, 1937). The geometric, kinematic and dynamic similarity between the model and the prototype is judged based on the analysis of acting forces, principal stresses, strains and rheological properties (elastic, viscous, plastic and brittle deformations or their combinations), for the model and prototype, respectively.

For geometric similarity, it must be true that the individual angles between surfaces in the deformed body of the prototype and the model are similar, while for the lengths, only the proportionality is necessary (e.g. Koyi, 1997). Relations between the length of the model and length of the prototype is:

$$\frac{l_n^m}{l_n^p}, \quad for \quad (n = 1, 2, 3..), \tag{1.1}$$

where l^m and l^p are the length of the model line or natural body line, respectively. For each n this ratio has to be identical and equality of angles between the lines must be guaranteed:

$$\alpha_n^p = \alpha_n^m, \quad \text{for} \quad (1, 2, 3..). \tag{1.2}$$

Another important scaling factor is the kinematic similarity, which is conditioned by geometric similarity and is proportional to the dimension of time (duration) required for development of the model and prototype, respectively. The time and relative linear velocities in the model, can then be determined by the following relationships (e.g. Hubbert, 1937 or Schellart and Strak, 2016):

$$\frac{t_n^m}{t_n^p}, \quad \text{for} \quad (1, 2, 3..), \tag{1.3}$$

$$v_p = v_m \frac{l^p t^m}{l^m t^p}. \tag{1.4}$$

Again, the ratio between model and prototype must be attained for all times n for these expressions.

Dynamic similarity is based on both geometric and kinematic similarity between the model and natural prototype. Here, the proportionality between forces acting on any point of the model and the real environment are considered. These forces are F_g (gravitational force), F_v (viscous force), F_p (tensile or compressive force), F_f

(frictional force) and possibly others (F_n). As in the previous case of geometric and kinematic similarity, have to be true that:

$$\frac{F_g^m}{F_g^p} = \frac{F_v^m}{F_v^p} = \frac{F_p^m}{F_p^p} = \frac{F_f^m}{F_f^p} = \frac{F_n^m}{F_n^p}, \tag{1.5}$$

wherein further (based on Cauchy equation of motion (Acheson, 1990) and Stokes' law (Stokes, 1851)) the following applies:

$$\frac{F^m}{F^p} = \frac{\rho^m (l^m)^3}{\rho^p (l^p)^3} = \frac{\Delta\rho^m (l^m)^3}{\Delta\rho^p (l^p)^3} \tag{1.6}$$

Here ρ is the density and for Earth's conditions is $g^m = g^p$.

1.3.1 Materials and rheology

A great variety of analogue materials can be used for analogue modelling, depending on the desired rheological properties (Fig. 3; Fig. 4) and the geometry of the prototype. Among the most widely used materials employed for tectonic analogue models of the upper crust and its brittle deformation are quartz sand (Fontainebleau sand) (Li, et al., 2013), glass microspheres (Schellart and Strak, 2016) or feldspar powder (Agostini et al, 2009). The scaling for the upper crustal strength is based on Byerlee's law (Byerlee, 1978), and for differential stress it can be expressed from the difference of maximum and minimum principal stress (Ranalli, 2000, Cagnard et al., 2006):

$$\sigma_1 - \sigma_3 = \frac{[2\mu\rho g z(1-\lambda) + 2S]}{[(\mu^2+1)^{1/2} - \mu]}, \tag{1.7}$$

where μ is the friction coefficient, ρ is the density, g is the gravitational acceleration, z is the thickness of the layer which is affected by brittle deformation, λ is the pore fluid factor and S is the cohesion factor of the used analogue material (specifically negligible for Fontainebleau sand).

The ductile deformation of the lower lithosphere includes several different subclasses of rheological models (Fig. 3), depending on the type of used material. These models combine elastic (transition to brittle deformation of the upper crust), plastic and viscous behavior of the material (Fig. 4) and are a prerequisite for a complex flow and deformation in the Earth's lithosphere. In the models that are associated with multi-layered domains (e.g. the upper and lower crust or salt and sedimentary cover - e.g. Brun, 2002; Brun and Fort, 2004) silicone putties are usually used for

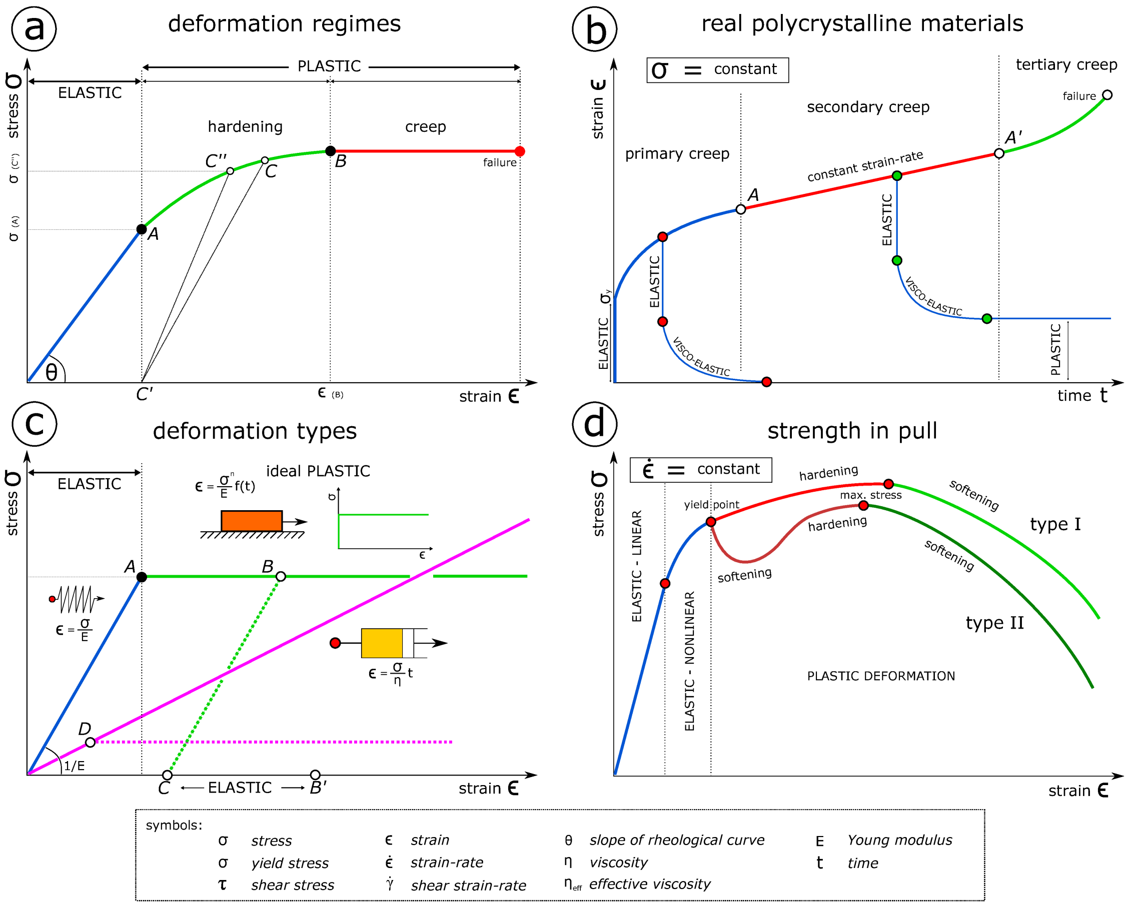

Fig. 3: Rheological relations and deformation regimes. Diagram (a) displays strain-stress relationship for polycrystalline rocks. The three elementary mechanical behavior regimes are characterized by elasto-visco-plastic deformation. A corresponds to the yield stress and change between elastic and plastic deformation, B-C segment represents hardened material after decreasing and repeatedly increasing of the stress (C→C'→C" hysteresis), and C represents the initiation of the creep when material is deformed under constant pressure. Slope of the elastic curve segment θ is related with $1/E$ (inverse Young's modulus). Diagram (b) displays a strain evolution in polycrystalline materials under constant applied stress. Diagram (c) represents the general overview of the basic rheological models for elastic, plastic and viscous deformation. Diagram (d) represents the strain-stress evolution of the materials in pull regime under the constant strain-rate where type I and type II curves differ in the rapid decreasing of the strength typically for different types of a crystalline/polycrystalline material. Diagrams (a-c) are modified after http://www.geosci.usyd.edu.au/users/prey/Teaching/ACSGT/Module1/Mod1LectPract/ and diagram (d) is modified after https://physics.mff.cuni.cz/kfpp/skripta/kurz_fyziky_pro_DS/.

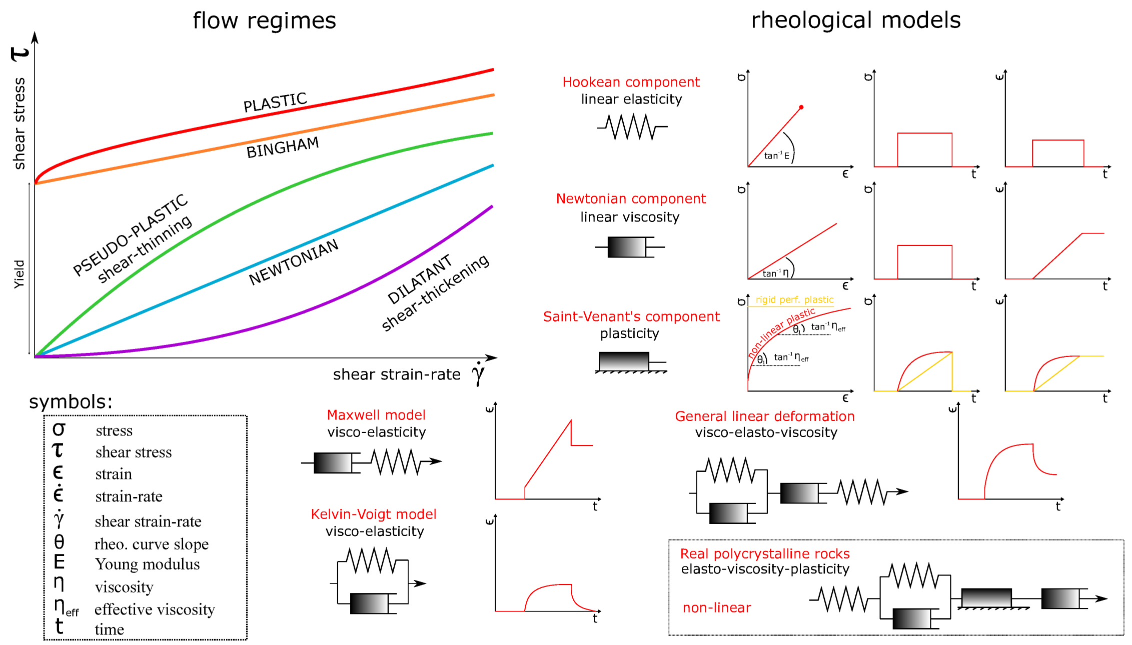

Fig. 4: Rheological models and flow regimes. The figure shows an overview of the general flow regimes in the shear-strain/stress diagram and the basic rheological models with basic interconnection to approximating the real rock behavior (strain-stress-time diagrams are modified after http://psgt.earth.lsa.umich.edu/PDF/2017/10_Lithosphere_2017.pdf).

ductile lower crust (Cagnard et al., 2006) and correspond to linear viscous Newtonian rheology. Ductile deformation (e.g. visco-plastic flow) of the more complex non-linear / power-law Non-Newtonian materials in the crust or mantle, can be alternatively simulated by plasticine (Pastor-Galán et al., 2012) or other materials undergoing the plastic (optionally viscous) deformation such as paraffine (Rossetti et al., 1999) or gelatine (visco-elasto-plastic deformation) (Kavanagh et al., 2013). Multi-layer models (that include e.g. the upper mantle and multilayered crust (e.g. Cagnard et al., 2006; Bajolet et al., 2015)) typically employ the same analogue material, only modified to match a specific density or viscosity for each successive layer. Thus, the correct scaling with respect to the prototype can still be justified, inspite of the fact that the linear and nonlinear rheology may not be appropriately scalable when used simultaneously in a single model. Different types of glucose syrups, glycerol solutions, heavy liquids etc are used for asthenosphere simulation (e.g. Mériaux et al., 2016, 2015; Schellart and Strak, 2016; Bajolet et al., 2015; Corti, 2012; Corti et al., 2003).

An overview of the relationships describing the visco-elasto-plastic deformation (including the viscous deformation and creep mechanisms, ductile flow or brittle deformation) can be found in Krýza (2013) or in Becker and Kaus, 2016; Ismail-Zadeh and Tackley (2010); Gerya (2009)

1.3.2 Scaling of a linear and non-linear rheology and flow properties

There are generally two approaches for scaling, depending on the rheological properties of employed analogue materials and dynamic properties of the flow. At geological time-scale and distances, the mechanism of viscous flow can be described by the creep relationship (e.g. Twiss and Moores, 2007):

$$\dot{\varepsilon} = A\sigma^n \exp\left(-\frac{E_A}{RT}\right), \tag{1.8}$$

where $\dot{\varepsilon}$ is the strain-rate, σ^n is the differential stress, E_A is the activation energy for creep, R is the Boltzman (gas) constant, T is the temperature and A is a material constant. Thus, linearly dependent strain (flux) can be scaled (e.q. Diffusion creep, Nabarro-Herring creep, Coble creep, where $n \sim 1$; Gerya, 2010) as well as non-linearly dependent strain (e.q. Dislocation creep, where $n > 1$).

To preserve the kinematic and dynamic similarity between the model and the prototype (see relations 1.3 - 1.6), it is necessary to match the parameters (dimensionless numbers) that control the equation of motion (Weijermars and Schmeling, 1986; Gerya, 2010) or derived equation of dynamics (Brun, 2002).

The equation of motion for a viscous medium (see subclass Navier-Stokes equations (e.q. Krýza, 2013)) can be expressed as follows (Weijermars and Schmeling, 1986):

$$\rho_0 \left(\frac{\partial v}{\partial t} + v \cdot \nabla v\right) = -\nabla p + \frac{\partial \tau_{ij}}{\partial x_j} + \rho g n_z, \tag{1.9}$$

where ρ is the density, v is the velocity, t is the time, p is the pressure, τ_{ij} is the shear stress, g is the gravitational acceleration and n_z is the unit vector along vertical direction. The driving parameters of the equation are following (Weijermars and Schmeling, 1986; Ramberg, 1981):

$$Re = \frac{vl\rho_0}{\eta}, \tag{1.10}$$

$$Sm = \frac{gl\rho_0}{\Delta p}, \tag{1.11}$$

$$St = \frac{l\Delta p}{\eta v}, \tag{1.12}$$

$$Rm = \frac{gl^2\rho_0}{\eta v}, \tag{1.13}$$

where $v, l, \rho, \eta, g, \Delta p$ are the velocity, length, density, viscosity, gravitational acceleration and pressure difference (*Re*: Reynolds number; *Sm*: Schmoluchowski number; *St*: Stokes number; *Rm*: Ramberg number). It can be shown that it is true that $Rm = S_t \cdot S_m$ and at the same time *Re* is extremely small for geological flows ($< 10 - 20$; Weijermars and Schmeling, 1986). Individual numbers can be interpreted as the following ratios: *Re* (inertia/viscous force), *Sm* (gravity/pressure gradient force), *St* (pressure gradient force/viscous force), *Rm* (gravity/viscous force).

So that the equation (1.9) becomes dimensionless and dimensionless variables can be used to characterize the relationship between the model and the prototype (linear rheology):

$$\begin{aligned}
\rho &= \rho'\rho_0, \\
r &= r'l, \\
t &= \frac{t'\eta_0}{\rho_0 g l}, \\
v &= \frac{v'\rho_0 g l^2}{\eta_0}, \\
\dot{e}_{ij} &= \frac{\dot{e}'_{ij}\rho_0 g l}{\eta_0}, \\
\tau_{ij} &= \tau'_{ij}\rho_0 g l, \\
p &= p'\rho_0 g l, \\
\nabla &= \nabla'/l, \\
\frac{\partial}{\partial t} &= \frac{\partial}{\partial t'}\frac{\rho_0 g l}{\eta_0},
\end{aligned} \tag{1.14}$$

where the scaling factor is marked by an apostrophe and scaling parameters are (l, ρ_0, η_0, g). These parameters express the dimensionless variables that can be substituted into the equation 1.9, which will change to:

$$\frac{gl^3\rho_0^2}{\eta_0^2}\left(\frac{\partial v'}{\partial t'} + v' \cdot \nabla' v'\right) = -\nabla' p' + \frac{\partial \tau'_{ij}}{\partial x'_j} + \rho' n_z, \tag{1.15}$$

where the scaling parameters are expressed on the left, while the right side shows dimensionless scaling factors. Since $Rm = St \cdot Sm$ and $Rm \cdot Re = gl^3\rho_0^2/\eta_0^2$ (or

$(Rm \cdot Re) \cdot L = R)$, it is possible to neglect the left side of equation (1.15) for $Re << 1$ and neglect the inertia forces (e.g. Buiter et al., 2016). Expression of dimensionless variables in the case of non-Newtonian viscous flow is following (eqs. 1.14 are the same as for the Newtonian flow):

$$
\begin{aligned}
t &= \frac{t'}{2^{n_0} A_0 l (lg\rho_0)^{n_0}}, \\
v &= v' 2^{n_0} A_0 l (lg\rho_0)^{n_0}, \\
\dot{e}_{ij} &= \dot{e}'_{ij} 2^{n_0} A_0 (lg\rho_0)^{n_0}, \\
\frac{\partial}{\partial t} &= \frac{\partial}{\partial t'} 2^{n_0} A_0 (lg\rho_0)^{n_0},
\end{aligned}
\tag{1.16}
$$

where A and n represent the material constant (empirically determined; e.g. by Carter, 1976; Kirby, 1983; Ranalli, 1997) and power of the non-linear behavior.

Based on the above relationships, the model can be directly scaled with respect to the real natural situation (prototype). The following relationships are given for both linear and non-linear viscous flow (Weijermars and Schmeling, 1986):

Linear

$$
\begin{aligned}
\rho_N &= \frac{\rho_{0N}}{\rho_{0M}} \rho_M, \\
r_N &= \frac{l_N}{l_M} r_M, \\
t_N &= \frac{\eta_{0N}}{\eta_{0M}} \left(\frac{\rho_{0M} g_M l_M}{\rho_{0N} g_N l_N} \right) t_M, \\
v_N &= \frac{\eta_{0M}}{\eta_{0N}} \left(\frac{\rho_{0N} g_N l_N^2}{\rho_{0M} g_M l_M^2} \right) t_M, \\
\dot{\gamma}_N &= \frac{\eta_{0M}}{\eta_{0N}} \left(\frac{\rho_{0N} g_N l_N}{\rho_{0M} g_M l_M} \right) \dot{\gamma}_M, \\
\tau_N &= \frac{\rho_{0N} g_N l_N}{\rho_{0M} g_M l_M} \tau_M, \\
p_N &= \frac{\rho_{0N} g_N l_N}{\rho_{0M} g_M l_M} p_M,
\end{aligned}
\tag{1.17a}
$$

Non-linear

$$
\begin{aligned}
t_N &= \frac{A_{0M}}{A_{0N}} \left(\frac{\rho_{0M} g_M l_M}{\rho_{0N} g_N l_N}\right)^{n_{0M}} t_M, \\
v_N &= \frac{A_{0N}}{A_{0M}} \left(\frac{\rho_{0M} g_M l_M}{\rho_{0N} g_N l_N}\right)^{n_{0M}} \frac{l_N}{l_M} v_M, \\
\dot{\gamma}_N &= \frac{A_{0N}}{A_{0M}} \left(\frac{\rho_{0N} g_N l_N}{\rho_{0M} g_M l_M}\right)^{n_{0M}} \dot{\gamma}_M,
\end{aligned}
\tag{1.17b}
$$

where $\gamma = 2\dot{\varepsilon}$ is the engineering strain-rate.

The scaling laws, including local variations of scaling relationships in inhomogeneous media, are described in detail by Weijermars and Schmeling (1986). The scaling relationships for dynamic similarity between the model and prototype with conservation of the equation of dynamics was also analyzed by Brun (2002). The thermal scaling relationships in analogue models were developed by Katz et al. (2005), Rossetti et al (1999) or Cobbold and Jackson (1992).

1.3.3 Artificial gravitational field

In models, where the effect of gravity on a material flow is crucial, the gravitational acceleration must be scaled. Such models are typical, for example, for gravitational inversion of the Earth's crustal materials (e.g. Dixon and Summers, 1983; Acocella et al., 2000; Godin et al., 2011; Harris et al., 2012; Nikkilä et al., 2015; Faisal and Dixon, 2015) or mantle dynamics (Tentler, 2003; Connolly et al, 2009) in the form of diapirism or mantle plumes (Fig. 5a). The rheological properties of analogue materials, that are scaled for crustal-scale analogue models, are discussed e.g. by Waffle et al. (2016). Also, extensional tectonics modelling can be provided by simulated and scaled gravitational acceleration (e.g. Brune et al., 2017; Agostini et al., 2009, etc.) which is usually generated by a centrifuge (Fig. 5b). Another type of models allow to apply an artificial gravitational field applied to compressional apparatus used in centrifuge and to produce thrust faults or folds in combination with gravitational inversion (Liu and Dixon, 1990; Liu and Dixon, 1991; Dixon and Liu, 1992).

The magnitude of gravitational acceleration itself can be expressed as the relationship between the angular velocity ω, rotations per minute x and radial distance R between the element of the model domain and the rotational axis of the centrifuge:

$$
g_M = \omega^2 \cdot R \left(\frac{2\pi x}{60}\right)^2 R \quad [m/s]. \tag{1.18}
$$

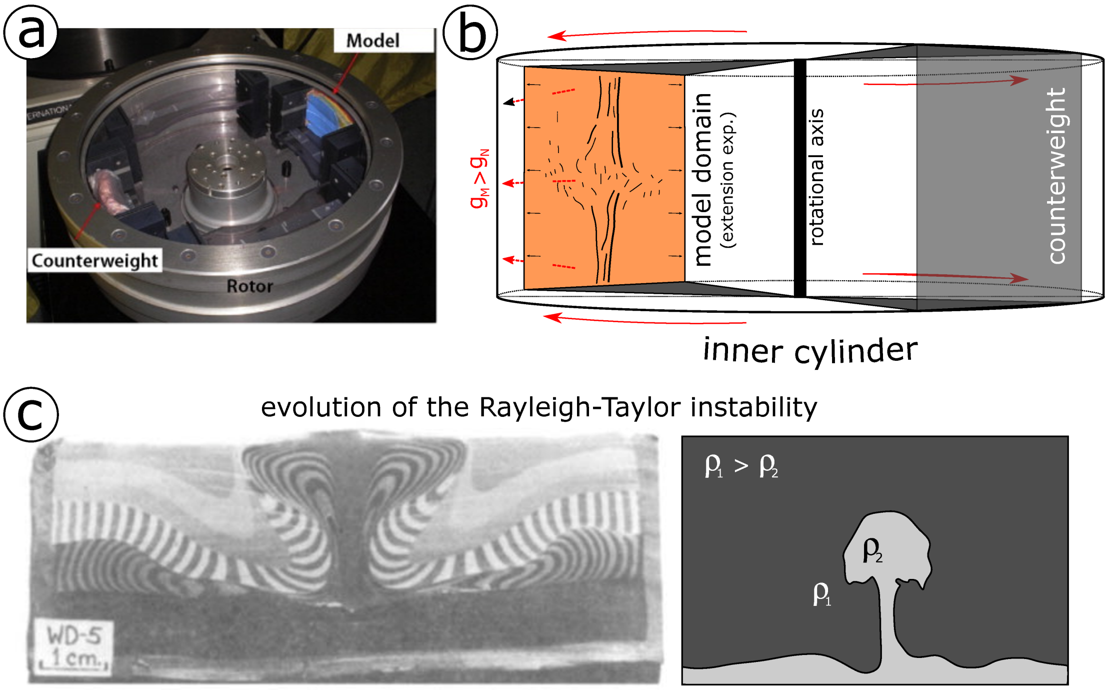

Fig. 5: Centrifuge modelling. Figure (a) displays the centrifuge device which is used for the geodynamical analogue modelling (taken from Harris et al., 2012). Schematic diagram(b) represents the principle of the centrifuge and simulation of the artificial gravitational field in the model domain (g_M). Example of the modelling with simulation of the Rayleigh-Taylor instability and gravitational inversion of the Earth's crust in the form of crustal-scale diapirs (*photo of the model is taken from Koyi (1997) according to experiments of Dixon (1974)*).

In this case, it should be noted that the Coriolis forces, which are insignificant in the case of solid-state flow of natural rock, also arise (Weijermars and Schmeling, 1986), however, they will play a significant role only for the low-viscosity models. Coriolis force damping effect of viscous forces is expressed by Taylor number (from equation of motion):

$$T_\alpha = \left(\frac{2\omega l^2 p_0}{\eta_0}\right)^2. \tag{1.19}$$

For any solid-state flow in geological conditions, it is true that $Re << 1$ and $T_\alpha << 1$ (Weijermars and Schmeling, 1986). The second way to simulate greater gravity, for example in slope motion models (Nolesini et al., 2013),development of accretionary wedges (Luján et al., 2010; Graveleau et al., 2012) or salt bodies (e.g. Weijermars et al., 1993), may be scaled for the inclination of a plane, on which the model is placed. In this case, the hydrostatic pressure value will be $h_M \cdot \rho_M \cdot g$ and the force F_g will be expressed for the inclination $\alpha_M > \alpha_N$. However, this way is not suitable for simulation of a material gravitational inversion such as e.g. formation and evolution of the Rayleigh-Taylor instabilities (Fig. 5c).

1.4 Recent analogue models of a large-scale mantle/lithosphere dynamics

During the last two decades, the technique and concepts of analogue models have advanced considerably allowing for simulation of more complex geodynamic processes. These models include both small scale processes (e.g. thrusting (Maillot and Koyi, 2006; Dotare et al., 2016), faulting (Mansfield and Cartwright; Corti et al., 2005), strike-slips (Rosas et al., 2015), water/magma/mud (channel-)flow (e.g. Mathieu et al., 2008; Mukherjee et al., 2012), pore fluid flow (Mourgues and Cobbold, 2016), erosion/sedimentation (Le Guerroué and Cobbold, 2006; Malavieille, 2010) etc.) and large-scale deformation of the lithosphere or mantle flow (e.g. subduction/rifting (Guillaume et al., 2009; Luth et al., 2010; Brune et al., 2017), salt diapirism (Warsitzka et al., 2013), mantle dynamics (Pysklywec and Cruden, 2004) and volcanic/magmatic processes (Martí et al., 2008; Gottsmann and Martí, 2011; Kavanagh et al., 2013)).

With the progressive development of photogrammetric methods and velocimetry (PIV), from the beginning of the 21st century, it is also possible to better quantify volume and surface changes and to obtain a deformation parameters based on $2D/3D$ velocity field (e.g. Adam et al., 2005). The implementation of these methods extends not only the possibility of deformation evaluation in the model domains, but also provides for higher scaling accuracy with respect to natural prototypes. For this reason, the application of the photogrammetry and the PIV is an integral part of this work.

1.5 Brief history and advances in the numerical geodynamic modelling

The beginning of approximate numerical methods in the broader sense can be dated back to the pre-Euclidean period. Simple methods for numerical solutions have also been widely used in ancient China and India. Compared to the ancient world, which was more concerned with the geometrical aspects of mathematics, the Asian-world scientists-philosophers dealt with algorithmization of calculations and the development of simple iterative numerical methods (e.g. Folta, 1988; Benzi, 2018 - online source).

During the modern history (from the 17th century), the ground for a more rigorous concept of numerical methods was gradually prepared as the infinitesimal mathematics developed. In connection with this period, we can mention a number of significant mathematicians who worked in the field of mathematical analysis and contributed to the foundations of modern numerical analysis (Newton, Euler, Lagrange, Gauss, Jacobi, Chebyschev, etc.). These mathematicians were in most cases natural scientists, and the application of mathematics was therefore offered in a number of disciplines, especially the physical ones (e.g. astronomy, hydrodynamics or engineering related problems). One of the first problems solved is an example of Isaac Newton's work: searching for a curved line of a parabolic type that can pass through a given number of points (polynomial of the nth order) mentioned in Book III, Lemma V (Newton, 1687).

Later, at the beginning of the 20th century, there were already specialized publications dealing with the specific development of a numerical solution of a number of scientific and technical problems (e.g. Whittaker and Robinson, 1924; Cassinis, 1928 or Longley, 1932). During this period, computers or handhelds were still not available for complex calculations and each computation is provided by hand calculations, slide rulers, desk calculators, electro-mechanical and other analogue devices (history can be found in Goldstine, 2012). The first computerized calculations were performed roughly between the 1930s and 1950s (Goldstine, 1980).

Modern numerical analysis was based on the concept of the Finite Difference Method (FDM) (Richardson, 1911; Courant and Lewy, 1928) developed during the 1960's -70's years, and contemporaneous with the development of the theory of plate tectonics. This revolution in geosciences was accompanied by definition of a range of new geodynamic problems (e.g. subduction models, models of the thermal and chemical mantle convection, a gravitational inversion of the crust etc.). The second major method which has been developed since the 1940's is the Finite Element Method (FEM) (e.g. Courant, 1943). This method is particularly suitable for the solution of partial differential equations in geometrically complex numerical domains. Development of this method marks the period of 1950 - 1970 and soon became another very important approach, widely used in geodynamics (from modelling of processes in the Earth's core, through the mantle and lithosphere dynamics to sedimentary processes).

From the beginning of the 70's until the end of the 1980, the most significant works representing the FDM and FEM calculations are following (list modified after Gerya, 2009):

- **1970:** *First 2D numerical models of subduction* (Minear and Toksoz, 1970). Purely thermal subduction model with prescribed corresponding velocity field (downgoing slab inclined at 45°).

- **1971:** *First 2D mantle thermal convection models* (Torrance and Turcotte, 1971). Possible implications for mantle convection with temperature-dependent viscosity for continental drift. Thermomechanical models based on the stream function formulation for the mechanical part were explored.

- **1972, 1978:** *First 2D numerical (FEM) models of salt dome dynamics* (Berner et al., 1972; Woidt, 1978). Until that moment, the geodynamic analogue modelling and analytical solutions were employed to investigate crustal diapirism only. Paper by Woidt (1978) discussed inconsistency of the numerical approach used by Berner et al. (1972).

- **1977-1980:** *First 2D mantle thermo-chemical convection modelling* (Keondzhyan and Monin, 1977, 1980). A binary stratified medium used to study the effects of compositional layering on mantle convection.

- **1978:** *First numerical models of continental collision* (Daignieres et al., 1978; Bird, 1978). Mechanical models exploring the finite-element approach.

- **1985-1986:** *First 3D spherical mantle convection models* (Baumgardner, 1985; Machetel et al., 1986). This first 3D models were spherical and not Cartesian.

- **1988:** *First 3D Cartesian mantle convection models* (Cserepes et al., 1988; Houseman, 1988).

With increasing computational potential, numerical modelling is nowadays a common part of complex geodynamic studies with wide application in plate tectonics. Key recent numerical models in the area of mantle and lithosphere dynamics and convergent tectonics will be discussed in appropriate chapters and sections.

1.6 Numerical solution and governing equations

The principle of a numerical approach is to solve an ordinary differential equation (ODE) or a partial differential equation (PDE) at discrete spatial distances or time steps. Thus, the solution is not a continuous analytical function, but a discrete function with a specific value at a particular space-time point, sharply separated from the surrounding space without an infinitesimal transition to the next point value. This approach is appropriate for very complex domains of interest where the key equations are addressed for 2D / 3D space with multiple boundary conditions and environmental properties (complex rheological models, complex heat transfer between subdomains, etc.) - as well as for equations whose analytical solution is nontrivial or is not possible to find it in reasonable time. In geoscience (geodynamic modelling), mainly the three governing equations are important: 1. Continuity equation (mass conservation); 2. Equations of motion (conservation of momentum); 3. Heat transfer equation (energy conservation).

1.6.1 Continuity equation

The continuity equation expresses the preservation of a quantity in a particular space-time element or volume. The basic derivation uses the divergence theorem (Gauss theorem):

$$\oint_{\Omega} \mathbf{A} \cdot \mathrm{d}\mathbf{S} = \int_{V} (\nabla \cdot \mathbf{A}) \mathrm{d}V, \tag{1.20}$$

where Ω is an enclosed surface which surrounds the volume V and which is oriented by the exterior normal vector $\mathrm{d}\mathbf{S} = \mathbf{n}\mathrm{dS}$ ($\mathbf{n}$ is the unit vector of the external normal vector), $\mathbf{A}$ is the vector field and ∇ is the nabla operator. The relation 1.20 expresses equality between the vector flux ($\mathbf{A}$) over the closed area and the volumetric integral of the vector $\mathbf{A}$ divergence (the flow across the boundary is equal to the sum of resources and sinks). This relationship can be used for scalar, vector and tensor quantities.

The continuity equation itself (derivation is possible to find e.g. in Krýza (2013)) then can be expressed in the Euler formulation (the point in the reference frame is fixed against the mobile environment) or in Lagrange formulation (the point of the mobile environment moves relative to the static reference frame). Both formulations of the continuity equation can be expressed (e.g. for density) as follows (e.g. Gerya, 2010):

Eulerian

$$\frac{\partial \rho}{\partial t} + \nabla \cdot (\rho \vec{v}) = 0, \tag{1.21}$$

Lagrangian

$$\frac{D\rho}{Dt} + \rho \nabla \cdot \vec{v} = 0, \tag{1.22}$$

where ρ is the density, $\vec{v}$ is the velocity and $\frac{D\rho}{Dt}$ is the material (Lagrange) derivative.

1.6.2 Momentum equation

The momentum conservation expresses the balance between the external and internal forces acting on a medium or body (continuum) in the gravitational field given by g. The effect and imbalance of these forces leads to the continuum deformation which can be described, for example, by Navier-Stokes equations for compressible or incompressible fluids. These equations are derived from the momentum equation by the relationship between the total stress (σ_{ij}) and deviatoric stress (σ'_{ij}) (e.g. Gerya, 2010; derivation is also possible to find in Ismail-Zadeh and Tackley (2010) or Krýza (2013)). The conservation of angular momentum itself can be expressed as follows (Lagrangian form):

$$\frac{\partial \sigma_{ij}}{\partial x_j} + \rho g_i = \rho \frac{D v_i}{Dt}. \tag{1.23}$$

Then the Navier-Stokes equations can be expressed from Cauchy momentum equation which contains the deviatoric stress tensor and pressure gradient:

$$\frac{\partial \sigma'_{ij}}{\partial x_j} - \frac{\partial P}{\partial x_i} + \rho g_i = \rho \frac{D v_i}{Dt}, \tag{1.24}$$

where P is the pressure (for the hydrostatic pressure is: $P = 1/3(xx + yy + zz)$). The Navier-Stokes momentum equation is then expressed as follows (convective formulation for compressible fluid):

$$\rho \frac{D\vec{v}}{Dt} = -\nabla \bar{p} + \mu \nabla^2 \vec{v} + \frac{1}{3}\mu \nabla (\nabla \cdot \vec{v}) + \rho g, \tag{1.25}$$

where ρ is the density of the fluid, μ is the fluid viscosity, $\vec{v}$ is the velocity and g is the gravitational acceleration.

1.6.3 Heat transfer equation

Another crucial equation is the heat transfer equation describing systems that include all known heat transfer mechanisms in the geological environment (advection, convection, conduction, radiation). In the integral form of the equation, it expresses the law of conservation of energy or the rate of change of energy E in the fixed volume of mass V. This change is equal to the sum of the work at the S boundary, the work produced by the external force F in a certain volume V, minus the heat which is transported internally by thermal conduction and convection, plus other heat sources (e.g. radiogenic heating, latent heat etc.). The equation can be written as follows (Ismail-Zadeh and Tackley, 2010):

$$\frac{\partial}{\partial t}\int_V \rho E \mathrm{d}\tau = \int_S v_i \sigma_{ij} \mathrm{d}S_j + \int_V \rho v_i F_i \mathrm{d}\tau - \int_S k \frac{\partial T}{\partial x_j} \mathrm{d}S_j - \int_S \rho E v_j \mathrm{d}S_j + \int_V \rho H \mathrm{d}\tau, \tag{1.26}$$

where t is the time, v is the velocity, T is the temperature, k is the conduction coefficient and H represents a heat sources (rate of the heat production, respectively).

The equation 1.26 can also be expressed in a differential form (Gerya, 2010) including the source terms H:

$$\rho C_P \frac{DT}{Dt} = -\frac{\partial q_i}{\partial x_i} + \sigma'_{ij} : \dot{\varepsilon}'_{ij} + T\alpha \frac{DP}{Dt} + H_L + H_r \quad (1.27)$$

where C_P is the heat capacity under the constant pressure, q is the heat flux (Fourier law), σ' is the deviatoric part of the stress tensor, $\dot{\varepsilon}'$ is the deviatoric part of the strain-rate tensor, P is the pressure and : is the double dot product symbol. The members on the right side of the equation represent (from the left) thermal conduction and heat sources such as: shear heating, adiabatic heating, latent heating (H_L) and radioactive heat production (H_r).

In addition to the conservation laws outlined above, other relationships relevant to a particular model situation, such as the isostatic compensation, erosion, sedimentation, phase transitions, chemical reactions, tidal effects or complex rheological models, play an important role (these model specifications were already described in Krýza (2013) and will not be described in detail in this thesis).

1.6.4 Numerical methods

In recent numerical mathematics, a large number of computational methods is available for a numerical solution of various types of partial differential equations. After designing the mathematical model which describe the specific area of interest, it is necessary to choose the most appropriate computational procedure. This method takes into account the geometry of the studied domain (and development of the convenient numerical grid) as well as optimized calculation of specific governing equations for current problem (Fig. 6).

Several different classes of numerical methods were developed, such as the Finite Difference Method (FDM)(e.g. Gerya, 2009; Grossmann et al., 2007), the Finite Element Method (FEM)(e.g. Becker and Kaus, 2016; Ismail-Zadeh and Tackley, 2010; Logan, 2011), the Finite Volume Method (FVM)(e.g. Ismail-Zadeh and Tackley, 2010; LeVeque, 2002; Eymard et al., 2000), spectral methods (e.g. Ismail-Zadeh and Tackley, 2010; Canuto et al., 2006), the Distinct Element Method (DEM)(e.g. Radjaï and Dubois, 2011; Munjiza, 2004), The Lattice Boltzmann Methods (LBM)(e.g. Mora and Yuen, 2017; Aharonov and Rothman, 1993) or the Numerical Manifold Method (NMM)(e.g. Wu and Wong, 2011; Ma et al., 2010). A short overview including applications and main advantages of these methods will be presented below.

FDM

The Finite Difference Method is one of the oldest numerical methods using a rectangular Eulerian grid. This approach using finite difference as direct approximation

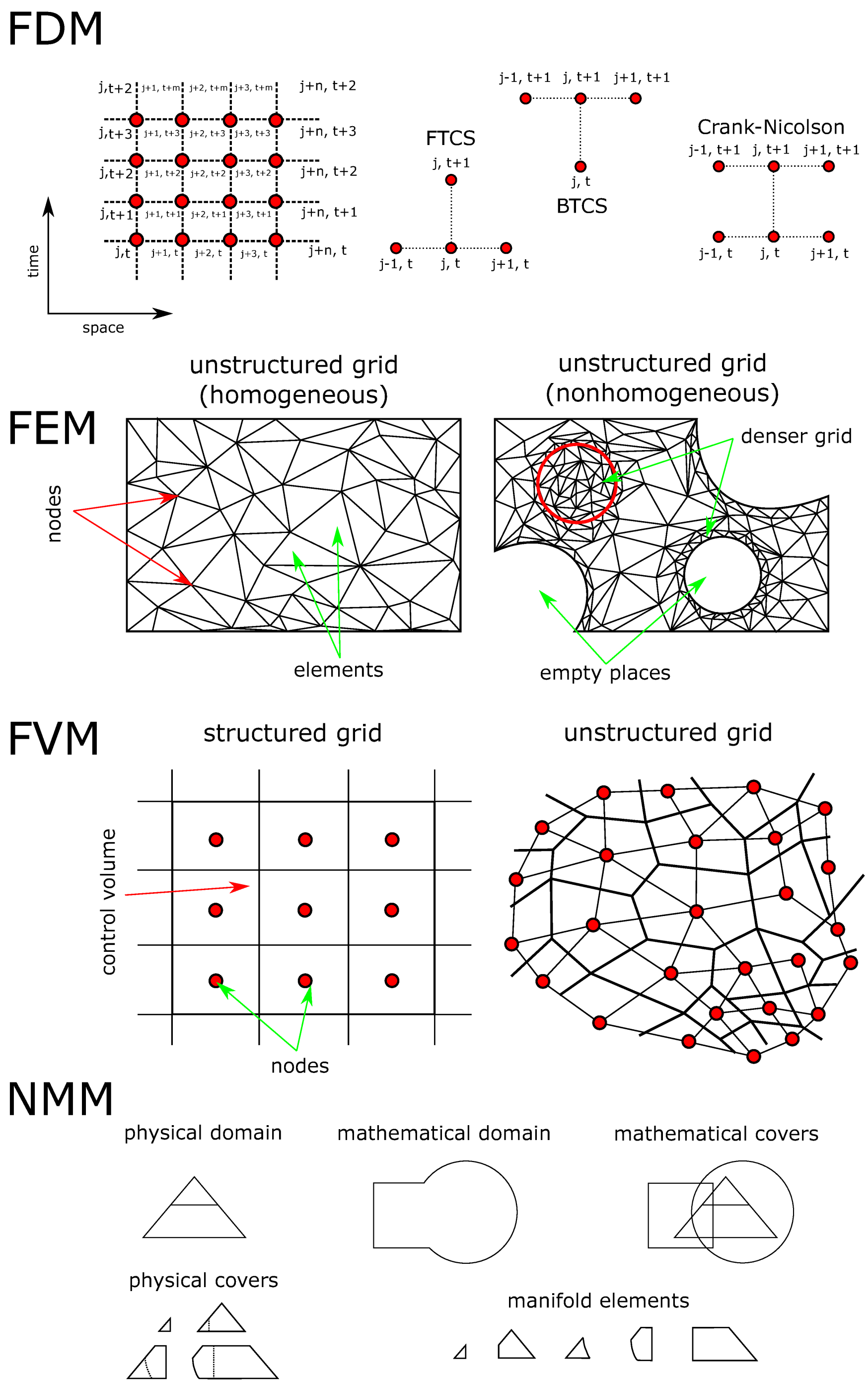

Fig. 6: Examples of the numerical grids for selected numerical methods. *The FVM grid scheme is modified after Ismail-Zadeh and Tackley (2010). The NMM domains and components are redrawn from Ma et al. (2010).*

and discretization of the differential equation. Each grid node then represents one finite difference member (respective derivative) from the series of the other differences that cover the whole model domain in a current time-step (Fig. 6). Discretization of the equation and the substitution of the derivatives by finite differences leads to the recurrent Euler scheme where a substituted system of algebraic equations is solved (Euler, 1768).

Generally, three basic calculation concepts are defined for algorithmization and determination of the finite differences (Fig. 6): 1. The explicit scheme - FTCS (Forward-Time Central-Space); 2. The implicit scheme - BTCS (Backward-Time Central-Space); 3. Crank-Nicolson scheme (combination of FTCS and BTCS schemes). The FTCS scheme represents the approach where the difference at the certain time t_n and second-order central space difference is used for calculation of the differences in t_{n-1} while BTCS scheme analogously using backward difference (i.e. the central space and time differences are expressed at t_{n-1} from differences at time t_n). For the FTCS scheme, the numerical stability (expressed by number of the numerical errors) is smaller than for BTCS scheme which is always numerically stable (BTCS scheme does not require any pre-condition for stability) and convergent. Numerical errors are proportional to the size of the time-step (linear over the time-step for the BTCS) and quadratically proportional to the space-step in both approaches. The Crank-Nicolson scheme is also always stable and convergent and both, time and space steps, are quadratic (Recktenwald, 2004).

FEM

The Finite Element Method represents one of the most common methods for solution of partial differential equations in wide spectra of computational applications. In contrast to the FEM, this method is not aimed to direct approximation of the system of the PDE. The core of the method is to convert the equation solution to the variational problem and to integrate the PDE in the whole model domain. The geometrically complex domain (Fig. 6) is divided into system of sub-domains (the finite elements) and solution of the PDE is substituted and approximated by polynomial function (contributed weight function) on each element. The set of these functions smoothly cover whole model domain and kind of their interlink determines the appropriate degree of local smoothness over the entire domain. The individual functions from each element then contribute to the variational integral. The resultant set of algebraic equations giving the approximate finite solution (in contrast to infinitesimal partial differential equation) as similar as in the FDM. In contrast to the FDM the discretization leads to approximate solution which is known in the form of polynomial functions and not set of isolated points.

For solutions where the advection transport of the material plays a key role, the Particle-In-Cell method is often employed together with the FEM (e.g. Wang et al., 2015). A similar approach is covered by implementation of the Marker-In-Cell method for FDM (e.g. Gerya and Yuen, 2003; Duretz et al., 2011b) where several factors are achieved by this technique, such as: 1. conservation of the stresses under conditions involving sharply discontinuous viscosity distribution; 2. heat and chemical composition conservation (non-linear transport coefficients, sharply variable conductivity or thermal gradients, etc); 3. Conservation of the scalar quantities with multiscale properties - e.g. thermal properties (thermal field), pressure properties, density in flows with strong advection (Gerya and Yuen, 2003).

FVM

The Finite Volume Method, which is also commonly used in geodynamic modelling, is similar to the FEM. The principle of the method is similar as in the case of the FEM but rather then elements, weight functions and variational integral, multiple control sub-volumes (Fig. 6) are used for discretization of the current equation. This equation is then integrated over each control volume where the volume integrals are converted to the surface integrals by using the divergence theorem (Gauss-Ostrogradsky Theorem)(e.g. Katz, 1979). Discretized equation then compare and equates the fluxes through control volumes respective to sources and sinks (divergence theorem) inside the current control volume. The solution of a discretized equation follows some of the standard methods for direct or iterative solution of the system of algebraic equations. This method can be easily used for unstructured grids as well as for regular Eulerian grids and thus the FVM combines advantages of both previously described methods (FDM and FEM).

Spectral methods

A principle of the spectral methods is similar to the FEM and FDM. However, in contrast to the FEM, FDM and FVM, the spectral methods using variables that are expanded as a sum of orthogonal global basis functions that are typically polynomial or trigonometric (nonzero basis functions through whole volume than in discrete element). The advantage of this method is that the convergence of the calculations is faster than for the above mentioned methods (spatial methods). High mathematical accuracy can be achieved for various spectra of models with simplified and smooth material and geometrical properties. This is provided by global prescription of the representative basis functions (that are local for spatial methods). These basis functions are typically different along prime directions - horizontal (azimuthal) and vertical (radial) - with respect to the differences in boundary conditions (e.g. periodicity of the side space boundary condition). As the basis functions can be easily used spherical harmonics and methods then became to be suitable for calculations of the problems defined in spherical geometry. The main disadvantage of this method is that for geometrically complicated domains, where sharp interfaces between material properties are implemented (sharp gradients are involved), the accuracy can rapidly decrease (Ismail-Zadeh and Tackley, 2010).

DEM

The Distinct Element Methods (or Discrete Element Methods) are characterized by using a large amount of discrete small particles that interact and simulate the effect of flow motion. The family of these methods is often used for geometrically complex model domains. However, rather than for complex rheological properties (combination of creeps and thermal flows) of the studied systems, the method is used to study granular flows and rock mechanics with more or less uniform composition. The advantage is that the method is well-designed to study brittle deformation (as development and propagation of joints, tears, faults, thrusts etc.) which is more difficult to approximate in the above mentioned methods. The starting point for implementation of the mentioned factors represents a combination of the DEM with the FEM (combined finite-discrete element method)(e.g. Lewis et al., 2005 or Gethin et al., 2006). The main disadvantage is that the method strongly depends on the amount of used particles and computational power (complex flows need to be simulated on computer clusters). Another disadvantage represents the complicated simulation of complex heat transfer in complicated domains where Lattice Boltzmann Method promises a more suitable approach.

LBM

The Lattice Boltzmann Method represents a relatively new technique for numerical simulations in computational fluid mechanics and geosciences. The principle of the method is to use a discrete mesh of fictitious particles that interact in sequential alternation of collision and streaming steps. Methods using a lattice Boltzmann equation apply discrete-velocity Boltzmann equations where the number of particles is decreased and the particles are confined by nodes of a lattice. The calculations of fluid density evolutions in current time and space coordinates produces multiple density components that are equal to the number of lattice vectors that are connected to each lattice point (Bao and Meskas, 2011).

The advantage of the method is that it is suitable for complex boundaries, geometries and porous media (and multiphase flows). Also the method is well designed to solve flow coupled with heat transfer and chemical reactions and can be effectively run on parallel architectures (parallel computing for large simulations). The main disadvantage and limitations are unduly small time steps for very small flows and potential errors related to artificial compressibility when the incompressible Navier-Stokes equations are solved (Bao and Meskas, 2011).

NMM

The Numerical Manifold Method is a relatively newly developed technique with applications mainly in modelling of strongly discontinuous features such as joints, faults, cracks etc (Zhang et al., 2010; Zhang et al., 1999; Ma et al., 2010).

Unlike FEM, where the model domain is divided into a set of elements (Fig. 6)(with a fixed number of nodes and vertices) and polynomial functions are used to establish unknown variables in an unknown field (by interpolation points and sets of algebraic equations), the approach of the NMM is based on physical and mathematical covers of the model domain with implementation of numerical manifolds. The method defines the physical domain (where an aimed physical problem is defined), mathematical domain (union of a finite number of patches - with potential to partly or totally overlap to each other - dividing the physical domain), mathematical cover (defined patches), physical covers (intersections of mathematical covers and physical domain) and manifold elements (defined as regions shared by several physical covers). The weight functions are formulated using an individual manifolds covering physical domain. Derivation of a weak form of governing equations then using the principle of virtual work and NMN interpolations are defined for each manifold. The discretized equations using element matrices that are assembled to form the system matrices based on the physical cover manifold topology. Similarly as in the FEM, the integration scheme uses individual elements. The manifolds represent general polygons (generalized shape of elements) that can be partitioned into variations of several triangles (depending on shape complexity) and integration scheme follows specific formulations using differential geometry relations. Generally, the FEM represents a special case of the FEM (Ma et al., 2010).

The overview of the numerical modelling components such as development of a Mathematical model, setting of the coordinate system, selection of a discretization method, numerical grid or convergence, stability and consistency criteria is described by Ismail-Zadeh and Tackley (2010).

The convergent and collisional tectonics represents complicated component of Earth dynamics which is associated with complex heat and material transfer. The regional scale models of the last decade revealed how various parameters (such as rheology, plate convergence rate, dip of subduction, geometry etc.) can affect specific heat and material distribution, phase processes, stress and deformation localization and P-T-t-d conditions (e.g. Podladchikov et al., 1993; Burg and Ford, 1997; Beaumont et al., 2001; Gerya et al., 2002; Beaumont et al., 2004; Duretz et al., 2011a; Tackley, 2012; Tackley et al., 2013; Gerya et al., 2015; Menant et al., 2016). Other models that are relevant for chapter IV of this study are presented in discussion sections.

1.7 Objectives of the research part of the thesis

Many of recent geodynamic research topics, where analogue modelling represents a native investigative component, is also combined with numerical modelling techniques. Similarly, in this work we combine both approaches. The core of the thesis is to study inner endogenic geodynamical processes as well as an exogenic dynamical processes at the surface of Earth and Mars. The two following chapters are aimed at the development and investigation of two analogue models representing oroclinal buckling and detachment folding. In chapter IV we present a numerical model of the crustal-scale Rayleigh-Taylor instability evolution (using FEM) while the chapters V and VI, are focused on simulations and studying of the Martian cryovolcanic mudflows (using analogue modelling, numerical approach combined with analytical calculations).

The second chapter of the thesis discusses the modelling and investigation of complex material flow and deformation in large accretionary systems associated with the development of large arcuate orogens such as the Tuva-Mongol orocline (e.g. Xiao et al., 2018, 2015), Cantabrian orocline (e.g. Li et al., 2018), Kazachstania orocline (e.g. Del Greco et al., 2016), etc.

The third chapter of the thesis is focused on the application of velocimetry and photogrammetry methods to advanced analogue indentation experiments (including detachment folding and oroclinal buckling). Here we find methods how to use the determined strain-related parameters and quantified material flux between specific model subdomains. In detachment folding experiments (e.g. Lehmann et al., 2017), we investigated the mechanism of melt ascent and injection along axial planes of developed folds. The model is aimed at describing complex dynamics of folding with dependence on time-space coordinates in a folded system.

In the fourth chapter of the thesis presents a numerical model where we study the effect of the Rayleigh-Taylor instability to crustal inversion and discuss the role of these instabilities in dynamics of indentation systems. The model is based on modelling approach used for development of orogenic root in Bohemian Massif during Brunia indentation (Maierová et al., 2014, 2012).

The fifth and sixth chapters are aimed at the investigation of mud behavior under Martian atmospheric conditions. The studied mudflows are related to cryovolcanic activity on Mars surface (e.g. Wilson and Mouginis-Mark, 2014). The analogue experiments are set to simulate pressure conditions at the Mars surface while gravity effects are discussed.

The major goals and questions of the thesis are:

- What is the mechanical interplay between oceanic and continental lithosphere during oroclinal buckling. How a general material transfer during this event is interlinked with deformation distribution/character and how this affects the global and local dynamics of these systems.
- What is the role of anatectic lower crust redistribution during indentation episode and regional-scale folding of the crust?

- How the rheological gradients and presence of light felsic lower crust affects the dynamics of collision systems? What is the role of Rayleigh-Taylor instability in the systems with various convergence rate?
- Do mudflows exist on the Mars surface? What is the dynamics of these cryovolcanism-based (potential) flows and which similarities they have with mud or lava flows that are developed on Earth?

1.8 References

Acheson, D. J. (1990). Elementary Fluid Dynamics. Oxford University Press. p. 205. ISBN 0-19-859679-0.

Acocella, V., Cifelli, F., and Funiciello, R. (2000). Analogue models of collapse calderas and resurgent domes. Journal of Volcanology and Geothermal Research, 104(1-4), 81-96.

Adam, J., Urai, J. L., Wieneke, B., Oncken, O., Pfeiffer, K., Kukowski, N., Lohrmann, J., Hoth, S., van der Zee, W. and Schmatz, J. (2005). Shear localisation and strain distribution during tectonic faulting—New insights from granular-flow experiments and high-resolution optical image correlation techniques. Journal of Structural Geology, 27(2), 283-301.

Adam, J., Klinkmüller, M., Schreurs, G., and Wieneke, B. (2013). Quantitative 3D strain analysis in analogue experiments simulating tectonic deformation: Integration of X-ray computed tomography and digital volume correlation techniques. Journal of Structural Geology, 55, 127-149.

Agostini, A., Corti, G., Zeoli, A., and Mulugeta, G. (2009). Evolution, pattern, and partitioning of deformation during oblique continental rifting: Inferences from lithospheric-scale centrifuge models. Geochemistry, Geophysics, Geosystems, 10(11).

Aharonov, E., and Rothman, D. H. (1993). Non-Newtonian flow (through porous media): A lattice-Boltzmann method. Geophysical Research Letters, 20(8), 679-682.

Bajolet, F., Galeano, J., Funiciello, F., Moroni, M., Negredo, A. M., and Faccenna, C. (2012). Continental delamination: Insights from laboratory models. Geochemistry, Geophysics, Geosystems, 13(2).

Bajolet, F., Replumaz, A., and Lainé, R. (2013). Orocline and syntaxes formation during subduction and collision. Tectonics, 32(5), 1529-1546.

Bajolet, F., Chardon, D., Martinod, J., Gapais, D., and Kermarrec, J. J. (2015).

Synconvergence flow inside and at the margin of orogenic plateaus: Lithospheric-scale experimental approach. Journal of Geophysical Research: Solid Earth, 120(9), 6634-6657.

Bao, Y. B., and Meskas, J. (2011). Lattice Boltzmann method for fluid simulations. Department of Mathematics, Courant Institute of Mathematical Sciences, New York University, 44.

Baumgardner, J. R. (1985) Three-dimensional treatment of convective flow in the Earth's mantle. Journal of Statistical Physics, 39, 501–11.

Beaumont, C., Jamieson, R. A., Nguyen, M. H., and Lee, B. (2001). Himalayan tectonics explained by extrusion of a low-viscosity crustal channel coupled to focused surface denudation. Nature, 414(6865), 738.

Beaumont, C., Jamieson, R. A., Nguyen, M. H., and Medvedev, S. (2004). Crustal channel flows: 1. Numerical models with applications to the tectonics of the Himalayan-Tibetan orogen. Journal of Geophysical Research: Solid Earth, 109(B6).

Becker, T. W., and Kaus, B. J. (2016). Numerical Modeling of Earth Systems. An introduction to computational methods with focus on solid Earth applications of continuum mechanics. University of Southern California, Los Angeles. Lecture notes (224 pages), available online at http://www-udc. ig. utexas. edu/external/becker/Geodynamics557. pdf, accessed, 9, 2017.

Benes, V., and Davy, P. (1996). Modes of continental lithospheric extension: experimental verification of strain localization processes. Tectonophysics, 254(1-2), 69-87.

Berner, H., Ramberg, H., and Stephansson, O. (1972). Diapirism theory and experiment. Tectonophysics, 15(3), 197-218.

Bird, P. (1978) Finite elements modeling of lithosphere deformation: The Zagros collision orogeny, Tectonophysics, 50, 307–36.

Boutelier, D. (2016). TecPIV—A MATLAB-based application for PIV-analysis of experimental tectonics. Computers and Geosciences, 89, 186-199.

Brun, J. P. (2002). Deformation of the continental lithosphere: Insights from brittle-ductile models. Geological Society, London, Special Publications, 200(1), 355-370.

Brun, J. P., and Fort, X. (2004). Compressional salt tectonics (Angolan margin). Tectonophysics, 382(3-4), 129-150.

Brune, S., Corti, G., and Ranalli, G. (2017). Controls of inherited lithospheric heterogeneity on rift linkage: Numerical and analog models of interaction between the Kenyan and Ethiopian rifts across the Turkana depression. Tectonics, 36(9), 1767-1786.

Burg, J. P., and Ford, M. (1997). Orogeny through time: an overview. Geological Society, London, Special Publications, 121(1), 1-17.

Buiter, S. J., Schreurs, G., Albertz, M., Gerya, T. V., Kaus, B., Landry, W., ... and Maillot, B. (2016). Benchmarking numerical models of brittle thrust wedges. Journal of structural geology, 92, 140-177.

Byerlee, J. (1978). Friction of rocks. In Rock friction and earthquake prediction (pp. 615-626). Birkhäuser, Basel.

Cadell, H. M. (1889) Experimental researches in mountain building Tans. R. Soc. Edinburgh, 1, pp. 339-343

Canuto, C., Hussaini, M. Y., Quarteroni, A., and Zang, T. A. (2006). Spectral methods. Springer-Verlag, Berlin.

Carter, N. L. (1976). Steady state flow of rocks. Reviews of Geophysics, 14(3), 301-360.

Cassinis G. (1928): Calcoli numerici grafici e meccanici. Mariotti – Pacini, Pisa.

Chemenda, A., Bouissou, S., and Bachmann, D. (2005). Three-dimensional physical modeling of deep-seated landslides: New technique and first results. Journal of Geophysical Research: Earth Surface, 110(F4).

Cloos, E. (1955). Experimental analysis of fracture patterns. Geological Society of America Bulletin, 66(3), 241-256.

Cobbold, P. R., and Jackson, M. P. A. (1992). Gum rosin (colophony): a suitable material for thermomechanical modelling of the lithosphere. Tectonophysics, 210(3-4), 255-271.

Colletta, B., Letouzey, J., Pinedo, R., Ballard, J. F., and Balé, P. (1991). Computerized X-ray tomography analysis of sandbox models: Examples of thin-skinned thrust systems. Geology, 19(11), 1063-1067.

Connolly, J. A., Schmidt, M. W., Solferino, G., and Bagdassarov, N. (2009). Permeability of asthenospheric mantle and melt extraction rates at mid-ocean ridges.

Nature, 462(7270), 209.

Corti, G. (2012). Evolution and characteristics of continental rifting: Analog modeling-inspired view and comparison with examples from the East African Rift System. Tectonophysics, 522, 1-33.

Corti, G., Moratti, G., and Sani, F. (2005). Relations between surface faulting and granite intrusions in analogue models of strike-slip deformation. Journal of Structural Geology, 27(9), 1547-1562.

Corti, G., Bonini, M., Conticelli, S., Innocenti, F., Manetti, P., and Sokoutis, D. (2003). Analogue modelling of continental extension: a review focused on the relations between the patterns of deformation and the presence of magma. Earth-Science Reviews, 63(3-4), 169-247.

Courant, R., Friedrichs, K. O., and Lewy, H. (1928) Über die partiellen Differenzengleichungen der mathematischen Physik, Mathematische Annalen 100, pp. 32

Courant, R. (1943). Variational methods for the solution of problems of equilibrium and vibrations. Verlag nicht ermittelbar.

Cserepes, L., Rabinowicz, M. and Rosemberg-Borot, C. (1988) Three-dimensional infinite Prandtl number convection in one and two layers and implications for the Earth's gravity field. Journal of Geophysical Research, 93, 12009–25.

Daignieres, M., Fremond, M. and Friaa, A. (1978) Modele de type Norton-Hoff généralisé pour l'étude des déformations lithosphériques (exemple: la collision Himalayenne), Comptes Reudus Hebdomadaires des Séances de l'Academie de Sciences, 268B, 371–74.

Daubre, A. (Dunod) (1879) Etudes synthétiques de géologie expérimentale, pt 1, Paris

Dauteuil, O., and Mart, Y. (1998). Analogue modeling of faulting pattern, ductile deformation, and vertical motion in strike-slip fault zones. Tectonics, 17(2), 303-310.

Davy, P., and Cobbold, P. R. (1988). Indentation tectonics in nature and experiment. 1. Experiments scaled for gravity. Bull. Geol. Inst. Univ. Uppsala, 14, 129-141.

Del Greco, K., Johnston, S. T., Gutiérrez-Alonso, G., Shaw, J., and Lozano, J. F. (2016). Interference folding and orocline implications: A structural study of the Ponga Unit, Cantabrian orocline, northern Spain. Lithosphere, 8(6), 757-768.

Dixon, J. M. (1974). A new method of determining finite strain in models of geological structures. Tectonophysics, 24(1-2), 99-114.

Dixon, J. M., and Summers, J. M. (1983). Patterns of total and incremental strain in subsiding troughs: experimental centrifuged. models of inter-diapir synclines. Canadian Journal of Earth Sciences, 20(12), 1843-1861.

Dixon, J. M., and Liu, S. (1992). Centrifuge modelling of the propagation of thrust faults. In Thrust tectonics (pp. 53-69). Springer, Dordrecht.

Dotare, T., Yamada, Y., Adam, J., Hori, T., and Sakaguchi, H. (2016). Initiation of a thrust fault revealed by analog experiments. Tectonophysics, 684, 148-156.

Duretz, T., Gerya, T. V., and May, D. A. (2011a). Numerical modelling of spontaneous slab breakoff and subsequent topographic response. Tectonophysics, 502(1-2), 244-256.

Duretz, T., May, D. A., Gerya, T. V., and Tackley, P. J. (2011b). Discretization errors and free surface stabilization in the finite difference and marker-in-cell method for applied geodynamics: A numerical study. Geochemistry, Geophysics, Geosystems, 12(7).

Escher, B. G., and Kuenen, P. H. (1928). Experiments in connection with salt domes. Leidse Geologische Mededelingen, 3(1), 151-182.

Euler, L. (1768). Institutiones Calculi Integralis, Vol. 1. Petersburg: Académie del Science (in French).

Eymard, R., Gallouët, T., and Herbin, R. (2000). Finite volume methods. Handbook of numerical analysis, 7, 713-1018.

Faisal, S., and Dixon, J. M. (2015). Physical analog (centrifuge) model investigation of contrasting structural styles in the Salt Range and Potwar Plateau, northern Pakistan. Journal of Structural Geology, 77, 277-292.

Favre, A. (1878a) Expériences sur les effets des refoulements ou écrasements latéraux en géologie Comptes Rendus Hebdomadaires des Séances de l'Académie des Sciences, pp. 1092-1095

Favre, A. (1878b) Expériences sur les effets des refoulements ou écrasements latéraux en géologie La Nature. Archives des sciences physiques et naturelles, 246 (1878), pp. 278-283

Folta, J. (1988). Some remarks on the history of Numerical Analysis especially in the area of Prague. Llull: Revista de la Sociedad Española de Historia de las Ciencias y de las Técnicas, 11(21), 217-234.

Galland, O., Bertelsen, H. S., Guldstrand, F., Girod, L., Johannessen, R. F., Bjugger, F., Burchardt, S. and Mair, K. (2016). Application of open-source photogrammetric software MicMac for monitoring surface deformation in laboratory models. Journal of Geophysical Research: Solid Earth, 121(4), 2852-2872.

Gerya, T. V., Stöckhert, B., and Perchuk, A. L. (2002). Exhumation of high-pressure metamorphic rocks in a subduction channel: A numerical simulation. Tectonics, 21(6), 6-1.

Gerya, T. (2009). Introduction to numerical geodynamic modelling. Cambridge University Press.

Gerya, T. V., and Yuen, D. A. (2003). Characteristics-based marker-in-cell method with conservative finite-differences schemes for modeling geological flows with strongly variable transport properties. Physics of the Earth and Planetary Interiors, 140(4), 293-318.

Gerya, T. V., Stern, R. J., Baes, M., Sobolev, S. V., and Whattam, S. A. (2015). Plate tectonics on the Earth triggered by plume-induced subduction initiation. Nature, 527(7577), 221.

Gethin, D. T., Yang, X. S., and Lewis, R. W. (2006). A two dimensional combined discrete and finite element scheme for simulating the flow and compaction of systems comprising irregular particulates. Computer methods in applied mechanics and engineering, 195(41-43), 5552-5565.

Godin, L., Yakymchuk, C., and Harris, L. B. (2011). Himalayan hinterland-verging superstructure folds related to foreland-directed infrastructure ductile flow: insights from centrifuge analogue modelling. Journal of Structural Geology, 33(3), 329-342.

Goldstine, H. H. (1980). The computer from Pascal to von Neumann. Princeton University Press.

Goldstine, H. H. (2012). A History of Numerical Analysis from the 16th through the 19th Century (Vol. 2). Springer Science and Business Media.

Gottsmann, J., and Martí, J. (Eds.). (2011). Caldera volcanism: analysis, modelling and response (Vol. 10). Elsevier.

Guillaume, B., Martinod, J., and Espurt, N. (2009). Variations of slab dip and overriding plate tectonics during subduction: Insights from analogue modelling. Tectonophysics, 463(1-4), 167-174.

Graveleau, F., Malavieille, J., and Dominguez, S. (2012). Experimental modelling of orogenic wedges: A review. Tectonophysics, 538, 1-66.

Griggs, D. T. (1939). A theory of mountain-building. American Journal of Science, 237(9), 611-650.

Grossmann, C., Roos, H. G., and Stynes, M. (2007). Numerical treatment of partial differential equations (Vol. 154). Berlin: Springer.

Hall Sir, J., 1805. Experiments on whinstone and lava. Trans. R. Soc. Edin. 5, 43–75.

Hall Sir, J., 1812. Account of a series of experiments, shewing the effects of compression in modifying the action of heat. Trans. R. Soc. Edin. 6, 71–185.

Hall Sir, J., 1815. On the vertical position and convolution of certain strata, and their relation with granite. Trans R. Soc. Edin. 7, 79–108.

Harris, L. B., Yakymchuk, C., and Godin, L. (2012). Implications of centrifuge simulations of channel flow for opening out or destruction of folds. Tectonophysics, 526, 67-87.

Houseman, G. (1988) The dependence of convection planform on mode of heating. Nature, 332, 346–9.

Hubbert, M. K. (1951) Mechanical basis for certain familiar geologic structures. Geol. Soc. Am. Bull., 62, pp. 355-372

Hubbert, M.K., 1937. Theory of scale models as applied to the study of geologic structures. Bull. Geol. Soc. Am. 48, 1459–1520.

Ismail-Zadeh, A., and Tackley, P. (2010). Computational methods for geodynamics. Cambridge University Press.

Jacoby, W. R. (1973). Model experiment of plate movements. Nature Physical Science, 242(122), 130.

Kavanagh, J. L., Menand, T., and Daniels, K. A. (2013). Gelatine as a crustal analogue: Determining elastic properties for modelling magmatic intrusions. Tectonophysics, 582, 101-111.

Katz, V. J. (1979). The history of Stokes' theorem. Mathematics Magazine, 52(3), 146-156.

Katz, R. F., Ragnarsson, R., and Bodenschatz, E. (2005). Tectonic microplates in a wax model of sea-floor spreading. New Journal of Physics, 7(1), 37.

Keondzhyan, V. P. and Monin, A. S. (1977) Continental drift and large-scale wandering of the Earth's pole. Izvestiya Physics of the Solid Earth, 13, 760–72.

Keondzhyan, V. P. and Monin, A. S. (1980) Compositional convection in the Earth's Mantle. Dokladi Akademii Nauk SSSR, 253, 78–81.

Kettermann, M., von Hagke, C., van Gent, H. W., Grützner, C., and Urai, J. L. (2016). Dilatant normal faulting in jointed cohesive rocks: a physical model study.

Kirby, S. H. (1983). Rheology of the lithosphere. Reviews of Geophysics, 21(6), 1458-1487.

Koyi, H. (1997). Analogue modelling: from a qualitative to a quantitative technique—a historical outline. Journal of Petroleum Geology, 20(2), 223-238.

Krýza, O. (2013) Application of the multivariate statistical methods for the analysis of the 2D thermo-mechanical numerical models of diapirism. Diploma thesis. Charles University, Prague.

Kuenen, P. H. (1936). The negative isostatic anomalies in the East Indies (with experiments). Leid. Geol. Med., 8, 169-214.

Le Guerroué, E., and Cobbold, P. R. (2006). Influence of erosion and sedimentation on strike-slip fault systems: insights from analogue models. Journal of Structural Geology, 28(3), 421-430.

Lehmann, J., Schulmann, K., Lexa, O., Závada, P., Štípská, P., Hasalová, P., ... and Corsini, M. (2017). Detachment folding of partially molten crust in accretionary orogens: A new magma-enhanced vertical mass and heat transfer mechanism. Lithosphere, 9(6), 889-909.

LeVeque, R. J. (2002). Finite volume methods for hyperbolic problems (Vol. 31). Cambridge university press.

Lewis, R. W., Gethin, D. T., Yang, X. S., and Rowe, R. C. (2005). A combined finite-discrete element method for simulating pharmaceutical powder tableting. International journal for numerical methods in engineering, 62(7), 853-869.

Li, Z., Escoffier, S., and Kotronis, P. (2013). Using centrifuge tests data to identify the dynamic soil properties: Application to Fontainebleau sand. Soil Dynamics and Earthquake Engineering, 52, 77-87.

Li, P., Sun, M., Rosenbaum, G., Yuan, C., Safonova, I., Cai, K., ... and Zhang, Y. (2018). Geometry, kinematics and tectonic models of the Kazakhstan Orocline, Central Asian Orogenic Belt. Journal of Asian Earth Sciences, 153, 42-56.

Liu, S. and Dixon, J. M. (1990). Centrifuge modelling of thrust faulting: strain partitioning and sequence of thrusting in duplex structures. Geological Society, London, Special Publications, 54(1), 431-444.

Liu, S. and Dixon, J. M. (1991). Centrifuge modelling of thrust faulting: structural variation along strike in fold-thrust belts. Tectonophysics, 188(1-2), 39-62.

Longley, W. R. (1932). JB Scarborough, Numerical Mathematical Analysis. Bulletin of the American Mathematical Society, 38(5), 331-332.

Logan, D. L. (2011). A first course in the finite element method. Cengage Learning.

Luján, M., Rossetti, F., Storti, F., Ranalli, G., and Socquet, A. (2010). Flow trajectories in analogue viscous orogenic wedges: Insights on natural orogens. Tectonophysics, 484(1-4), 119-126.

Luth, S., Willingshofer, E., Sokoutis, D., and Cloetingh, S. (2010). Analogue modelling of continental collision: influence of plate coupling on mantle lithosphere subduction, crustal deformation and surface topography. Tectonophysics, 484(1-4), 87-102.

Ma, G., An, X., and He, L. (2010). The numerical manifold method: a review. International Journal of Computational Methods, 7(01), 1-32.

Machetel, P., Rabinowicz, M. and Bernardet, P. (1986) Three-dimensional convection in spherical shells. Geophysical and Astrophysical Fluid Dynamics, 37, 57–84.

Maierova, P., Lexa, O., Schulmann, K., and Štípská, P. (2014). Contrasting tectonometamorphic evolution of orogenic lower crust in the Bohemian Massif: a numerical model. Gondwana Research, 25(2), 509-521.

Maierová, P., Čadek, O., Lexa, O., and Schulmann, K. (2012). A numerical model of exhumation of the orogenic lower crust in the Bohemian Massif during the Variscan orogeny. Studia Geophysica et Geodaetica, 56(2), 595-619.

Maillot, B., and Koyi, H. (2006). Thrust dip and thrust refraction in fault-bend folds: analogue models and theoretical predictions. Journal of Structural Geology, 28(1), 36-49.

Malavieille, J. (2010). Impact of erosion, sedimentation, and structural heritage on the structure and kinematics of orogenic wedges: Analog models and case studies. Gsa Today, 20(1), 4-10.

Mansfield, C., and Cartwright, J. (2001). Fault growth by linkage: observations and implications from analogue models. Journal of Structural Geology, 23(5), 745-763.

Martí, J., Geyer, A., Folch, A., and Gottsmann, J. (2008). A review on collapse caldera modelling. Developments in Volcanology, 10, 233-283.

Mathieu, L., De Vries, B. V. W., Holohan, E. P., and Troll, V. R. (2008). Dykes, cups, saucers and sills: Analogue experiments on magma intrusion into brittle rocks. Earth and Planetary Science Letters, 271(1-4), 1-13.

Mead, W. J. (1920) Notes on the mechanics of geologic structures J. Geol., 28, pp. 505-523

Menant, A., Sternai, P., Jolivet, L., Guillou-Frottier, L., and Gerya, T. (2016). 3D numerical modeling of mantle flow, crustal dynamics and magma genesis associated with slab roll-back and tearing: The eastern Mediterranean case. Earth and Planetary Science Letters, 442, 93-107.

Mériaux, C. A., Mériaux, A. S., Schellart, W. P., Duarte, J. C., Duarte, S. S., and Chen, Z. (2016). Mantle plumes in the vicinity of subduction zones. Earth and Planetary Science Letters, 454, 166-177.

Mériaux, C. A., Duarte, J. C., Duarte, S. S., Schellart, W. P., Chen, Z., Rosas, F., ... and Terrinha, P. (2015). Capture of the Canary mantle plume material by the Gibraltar arc mantle wedge during slab rollback. Geophysical Journal International, 201(3), 1717-1721.

Minear, J. W., and Toksöz, M. N. (1970). Thermal regime of a downgoing slab and new global tectonics. Journal of Geophysical Research, 75(8), 1397-1419.

Mora, P., and Yuen, D. A. (2017). Simulation of plume dynamics by the Lattice Boltzmann Method. Geophysical Journal International, 210(3), 1932-1937.

Mourgues, R., and Cobbold, P. R. (2006). Thrust wedges and fluid overpressures: Sandbox models involving pore fluids. Journal of Geophysical Research: Solid Earth, 111(B5).

Mukherjee, S., Koyi, H. A., and Talbot, C. J. (2012). Implications of channel flow analogue models for extrusion of the Higher Himalayan Shear Zone with special reference to the out-of-sequence thrusting. International Journal of Earth Sciences, 101(1), 253-272.

Munjiza, A. A. (2004). The combined finite-discrete element method. John Wiley and Sons.

Newton, I. (1687). Philosophiae Naturalis Principia Mathematica.

Nikkilä, K., Korja, A., Koyi, H., and Eklund, O. (2015). Analog modeling of one-way gravitational spreading of hot orogens–A case study from the Svecofennian orogen, Fennoscandian Shield. Precambrian Research, 268, 135-152.

Nolesini, T., Di Traglia, F., Del Ventisette, C., Moretti, S., and Casagli, N. (2013). Deformations and slope instability on Stromboli volcano: Integration of GBInSAR data and analog modeling. Geomorphology, 180, 242-254.

Parker, T. J., and McDowell, A. N. (1955). Model studies of salt-dome tectonics. AAPG Bulletin, 39(12), 2384-2470.

Pastor-Galán D., Gutiérrez-Alonso G., Zulauf G. and Zanella F. (2012) Analogue modeling of lithospheric-scale orocline buckling: Constraints on the evolution of the Iberian-Armorican Arc. Geological Society of America Bulletin, 124, 1293-1309.

Podladchikov, Y., Talbot, C., and Poliakov, A. N. B. (1993). Numerical models of complex diapirs. Tectonophysics, 228(3-4), 189-198.

Pysklywec, R. N., and Cruden, A. R. (2004). Coupled crust-mantle dynamics and intraplate tectonics: Two-dimensional numerical and three-dimensional analogue modeling. Geochemistry, Geophysics, Geosystems, 5(10).

Radjaï, F., and Dubois, F. (2011). Discrete-element modeling of granular materials (pp. 425-p). Wiley-Iste.

Ramberg, H. (1981). Gravity, deformation, and the earth's crust: In theory, experiments, and geological application. Academic press.

Ramberg, H. (1970). Model studies in relation to intrusion of plutonic bodies, in: Newall, G., Rast, N. (Eds.), Mechanism of igneous intrusion, 2 ed, pp. 261–286

Ramberg, H. (1964). Selective buckling of composite layers with contrasted rheological properties, a theory for simultaneous formation of several orders of folds. Tectonophysics, 1(4), 307-341.

Ramberg, H. (1955). Natural and experimental boudinage and pinch-and-swell structures. The Journal of Geology, 63(6), 512-526.

Ranalli, G. (2001). Experimental tectonics: from Sir James Hall to the present. Journal of Geodynamics, 32(1-2), 65-76.

Ranalli, G. (2000). Rheology of the crust and its role in tectonic reactivation. Journal of geodynamics, 30(1-2), 3-15.

Ranalli, G. (1997). Rheology of the lithosphere in space and time. Geological Society, London, Special Publications, 121(1), 19-37.

Recktenwald, G. W. (2004). Finite-difference approximations to the heat equation. Mechanical Engineering, 10, 1-27.

Richardson, L. F. (1911). IX. The approximate arithmetical solution by finite differences of physical problems involving differential equations, with an application to the stresses in a masonry dam. Philosophical Transactions of the Royal Society of London. Series A, Containing Papers of a Mathematical or Physical Character, 210(459-470), 307-357.

Rosas, F. M., Duarte, J. C., Schellart, W. P., Tomás, R., Grigorova, V., and Terrinha, P. (2015). Analogue modelling of different angle thrust-wrench fault interference in a brittle medium. Journal of Structural Geology, 74, 81-104.

Rossetti, F., Ranalli, G., and Faccenna, C. (1999). Rheological properties of paraffin as an analogue material for viscous crustal deformation. Journal of Structural Geology, 21(4), 413-417.

Schellart, W. P., and Strak, V. (2016). A review of analogue modelling of geodynamic processes: Approaches, scaling, materials and quantification, with an application to subduction experiments. Journal of Geodynamics, 100, 7-32.

Schreurs, G., Buiter, S. J., Boutelier, D., Corti, G., Costa, E., Cruden, A. R., ... and Lohrmann, J. (2006). Analogue benchmarks of shortening and extension experiments. Special Publication-Geological Society of London, 253, 1.

Schreurs, G., Buiter, S. J., Boutelier, J., Burberry, C., Callot, J. P., Cavozzi, C., ... and Cruz, L. (2016). Benchmarking analogue models of brittle thrust wedges. Journal of structural geology, 92, 116-139.

Stokes, G. G. (1851). "On the effect of internal friction of fluids on the motion of pendulums". Transactions of the Cambridge Philosophical Society. 9, part ii: 8–106.

Strak, V., and Schellart, W. P. (2014). Evolution of 3-D subduction-induced mantle flow around lateral slab edges in analogue models of free subduction analysed by stereoscopic particle image velocimetry technique. Earth and Planetary Science Letters, 403, 368-379.

Tackley, P. J., Ammann, M., Brodholt, J. P., Dobson, D. P., and Valencia, D. (2013). Mantle dynamics in super-Earths: Post-perovskite rheology and self-regulation of viscosity. Icarus, 225(1), 50-61.

Tackley, P. J. (2012). Dynamics and evolution of the deep mantle resulting from thermal, chemical, phase and melting effects. Earth-Science Reviews, 110(1-4), 1-25.

Tapponnier, P., Peltzer, G., Le Dain, A. Y., Armijo, R., and Cobbold, P. (1982). Propagating extrusion tectonics in Asia: New insights from simple experiments with plasticine. Geology, 10(12), 611-616.

Tentler, T. (2003). Analogue modeling of overlapping spreading centers: insights into their propagation and coalescence. Tectonophysics, 376(1-2), 99-115.

Torrance, K. E. and Turcotte, D. L. (1971) Thermal convection with large viscosity variations. Journal of Fluid Mechanics, 47, 113–25.

Twiss, R. J., and Moores, E. M. (2007). Structural geology (2nd ed., 736 p). New York: W. H. Freeman and Company

Waffle, L., Godin, L., Harris, L. B., and Kontopoulou, M. (2016). Rheological and physical characteristics of crustal-scaled materials for centrifuge analogue modelling. Journal of Structural Geology, 86, 181-199.

Wang, H., Agrusta, R., and van Hunen, J. (2015). Advantages of a conservative velocity interpolation (CVI) scheme for particle-in-cell methods with application in geodynamic modeling. Geochemistry, Geophysics, Geosystems, 16(6), 2015-2023.

Warsitzka, M., Kley, J., and Kukowski, N. (2013). Salt diapirism driven by differential loading—Some insights from analogue modelling. Tectonophysics, 591, 83-97.

Warsitzka, M., Kukowski, N., and Kley, J. (2017, April). Kinematics and dynamics of salt movement driven by sub-salt normal faulting and supra-salt sediment accumulation-combined analogue experiments and analytical calculations. In EGU General Assembly Conference Abstracts (Vol. 19, p. 9213).

Weijermars, R., and Schmeling, H. (1986). Scaling of Newtonian and non-Newtonian fluid dynamics without inertia for quantitative modelling of rock flow due to gravity (including the concept of rheological similarity). Physics of the Earth and Planetary Interiors, 43(4), 316-330.

Weijermars, R. M. P. A., Jackson, M. T., and Vendeville, B. (1993). Rheological and tectonic modeling of salt provinces. Tectonophysics, 217(1-2), 143-174.

Whitehead Jr, J. A., and Luther, D. S. (1975). Dynamics of laboratory diapir and plume models. Journal of Geophysical Research, 80(5), 705-717.

Whittaker, E. T., and Robinson, G. (1924). The calculus of observations: a treatise on numerical mathematics. The calculus of observations.

Willis, B. (1893) Part 2; The Mechanics of Appalachian Structure United States Geological Survey Annual Report 13 (1893), pp. 211-281 (Part 2)

Wilson, L., and Mouginis-Mark, P. J. (2014). Dynamics of a fluid flow on Mars: Lava or mud?. Icarus, 233, 268-280.

Woidt, W. D. (1978) Finite-element calculations applied to salt dome analysis. Tectonophysics, 50 (2–3), 369–86.

Wu, Z., and Wong, L. N. Y. (2012). Frictional crack initiation and propagation analysis using the numerical manifold method. Computers and Geotechnics, 39, 38-53.

Xiao, W., Windley, B. F., Han, C., Liu, W., Wan, B., Zhang, J. E., ... and Song, D. (2018). Late Paleozoic to early Triassic multiple roll-back and oroclinal bending of the Mongolia collage in Central Asia. Earth-Science Reviews, 186, 94-128.

Xiao, W., Windley, B. F., Sun, S., Li, J., Huang, B., Han, C., ... and Chen, H. (2015). A tale of amalgamation of three Permo-Triassic collage systems in Central Asia: oroclines, sutures, and terminal accretion. Annual review of earth and planetary sciences, 43, 477-507.

Xu, Q., Zhao, Y., Hou, T., Wang, J., Zhao, X., Liu, J., and Wang, D. (2018). The evolution of folds-thrust wedges: Mathematical simulation based on finite difference method. Journal of Intelligent and Fuzzy Systems, 34(2), 1071-1081.

Zhang, G. X., Sugiura, Y., and Saito, K. (1999). Application of manifold method to jointed dam foundation. In Proc. Third Int. Conf. Analysis of Discontinuous Deformation (ICADD-3) (pp. 211-220).

Zhang, H. H., Li, L. X., An, X. M., and Ma, G. W. (2010). Numerical analysis of 2-D crack propagation problems using the numerical manifold method. Engineering analysis with boundary elements, 34(1), 41-50.

Zwaan, F., and Schreurs, G. (2017). How oblique extension and structural inheritance influence rift segment interaction: Insights from 4D analog models. Interpretation, 5(1), SD119-SD138.

Internet sources

http://geologypics.com/geological-item/brittle-structures-photos/ (11.2.2019)

https://physics.mff.cuni.cz/kfpp/skripta/kurz_fyziky_pro_DS/display.php/kontinuum/2 (12.2.2019)

http://psgt.earth.lsa.umich.edu/PDF/2017/10_Lithosphere_2017.pdf (12.2.2019)

http://www.geosci.usyd.edu.au/users/prey/Teaching/ACSGT/Module1/Mod1LectPract/Sld025.htm (20.2.2019)

Benzi, M. http://www.mathcs.emory.edu/~benzi/andhttp://history.siam.org/5C/pdf/nahist_Benzi.pdf (28.12. 2018)

List of abbreviations

2D - two dimensional
3D - three dimensional
DEM - Discrete/distinct Element Method
FDM - Finite Difference Method
FEM - Finite Element Method
FVM - Finite Volume Method
LBM - Lattice Boltzmann Method
NMM - Numerical Manifold Method
ODE - ordinary differential equation
PDE - partial differential equation
SM - spectral method

Part II

Mass and heat transfer in the accretionary systems

2 Oroclinal buckling and associated lithospheric-scale material flow

Ondřej Krýza, Ondrej Lexa, Karel Schulmann, Alexandra Guy, Denis Gapais, John Cosgrove and Wenjio Xiao

2.1 Abstract

We present a new analogue model of oroclinal buckling which is based on recent advances in our understanding of the giant Mongolian orocline in central Asia. The model simulates an amplification of a preexisting, gently folded, accretionary system represented by oceanic crust relaminated by felsic material separated from the oceanic lithosphere by a continental ribbon above a subduction zone. Consequently, in the analogue model we established two neighboring subdomains that represent continental and oceanic domains separated by a steep elastic "subduction" interface. The orthogonal shortening of the model domain, which is parallel to the pseudo-linear interface between these subdomains, produces two different deformation patterns in the orocline amplified interlimb areas. We used a standard modeling techniques to investigate both, flow of a ductile lithosphere and brittle deformation of an upper crust that are associated with orocline development. The modelling results show that: (1) two types of regional-scale folds develop, including the steeply plunging orocline and upright folds with horizontal hinges, (2) the overall deformation distribution shows significant thickening/thinning and exhumation of lower ductile layers with variations in dependence on the distance from the piston, (3) the finite geometry of the lithosphere is strongly contrasting in both oceanic and continental orocline hinge sectors, (4) the geometry of orocline is non-cylindrical with increasing plunge of the fold axis from upper crust towards deeper lithospheric layers. The model results are used to explain geophysically constrained deep crustal structure and surface deformation pattern of the Mongolia orocline.

Keywords: Analogue modelling, Tuva-Mongol orocline, oroclinal buckling, indentation

Highlights:

- Oroclinal buckling model of vertical belt separating horizontally stratified domains
- Early buckling stage shows characteristic of indentation tectonics
- Orocline amplification causes large scale vortex flow around inflection line

2.2 Introduction

The three-dimensional character of orogenic systems has long been recognized and studied by a range of authors (e.g. Şengör, 1993). However, commonly, the geodynamic evolution of orogenic systems has been presented perpendicular to the orogenic belt using two-dimensional cross-sections, as this is the plane in which most of material transfers occur. Similarly, most existing numerical models of continental collision and/or oceanic subduction are two-dimensional. Even if these models are very successful in simulating the main features of orogenic processes, they are no substitute for the fully scaled, 3D modeling required to examine the role of the systems mechanical anisotropy and material flow which also occurs along the strike of the belt. 3D numerical modeling of such systems is considerably sophisticated, difficult for programming and time-consuming (Gerya and Stöckhert, 2006; Gerya, 2014; Maierová et al., 2012, 2014 and 2018). It was therefore decided to study the behavior of these systems under laboratory conditions via analogue modeling.

The simulation of the oroclinal buckling of orogenic systems requires a 3D approach because the material flows both laterally and vertically during deformation (Pastor-Galán et al., 2012). Oroclinal bending affects linear orogenic systems located between oceanic lower plate and oceanic or continental upper plate either by passive oroclinal bending (e.g. Menant et al., 2016; Rosenbaum and Lister, 2004; Rosenbaum, 2012) or active oroclinal bending and buckling (Edel et al., 2014; Lehmann et al., 2010; Rosenbaum, 2014; Weil et al., 2001). The passive bending mode is uniquely controlled by the geometry of the subducting plate such as curvatures produced by variations in rollback velocity (Fig. 7a). In contrast, active oroclinal bending is controlled by horizontal indentation perpendicular to the subduction/accretionary orogen (e.g. the entry of an oceanic plateau or a continental block into a subduction zone) or high localized friction producing elevated and localized interplate coupling between the subducting plate and forearc region (Boutelier et al., 2014). In contrast, oroclinal buckling results from buckling instability during the orogen-parallel shortening of a linear orogenic belt (Fig. 7a and b) between two continental blocks (Lehmann et al., 2010; Edel et al., 2014). Recent analogue modeling of Boutelier et al., (2019) showed that the oroclinal buckling occurs during pull of continental ribbon by subduction and simultaneous extension forming a back-arc domain. In their model, both passive bending and buckling modes enhance each other occur simultaneously, which is the preferred model of Xiao et al. (2018) to explain deformation pattern of the central Asian oroclines.

Oroclinal buckling tectonics, the topic of this study, can be considered as a specific type of indentation tectonics accompanied by lateral movements of oroclinal hinges perpendicular to the movements of continental blocks. The whole process of oroclinal buckling depends on a number of factors including: the lateral surface curvature of the accretionary belt, variations in geometry and thickness of the upper and lower plate, variations in rheology and thermal state of both interacting plates and the evolution of the lithosphere after slab break-off (e.g. Menant et al., 2016). In

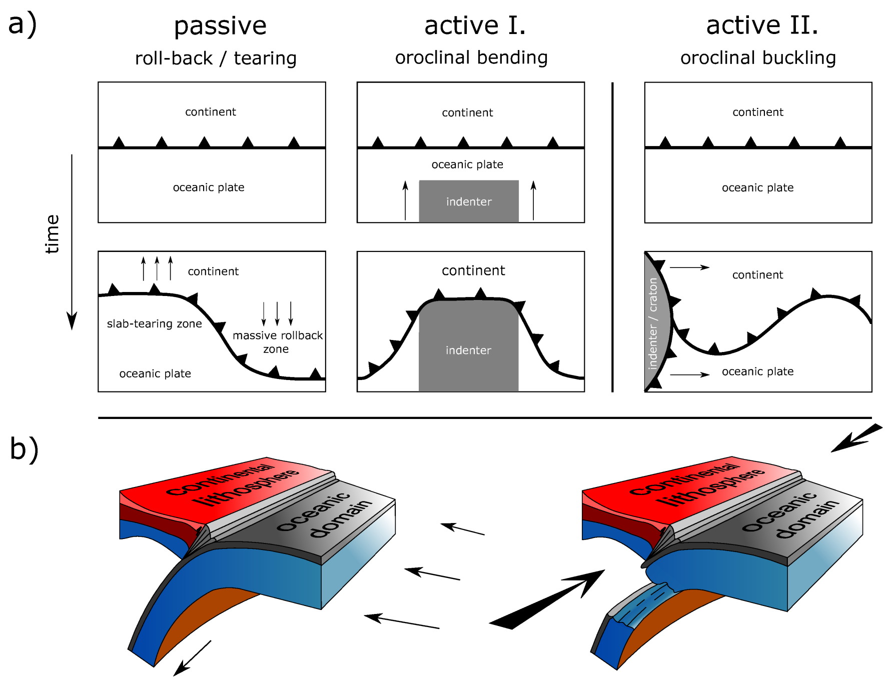

Fig. 7: Illustration of the mechanisms responsible for oroclinal arcuating. Three different basic styles of arcuating (passive/active) of the orogens are shown in (a). Passive arcuating is related to laterally asymmetrical progressive subduction where asymmetrical roll-back is developed by one-side tearing of the sinking slab. The first class active arcuating (bending) is produced by indentation tectonics where a microcontinent is embedded into a continental block while the indentation tectonics forms a gently curved contact line. The second class active arcuating (buckling) is a product of lateral accretion of a lithospheric block (e.g. cratonic part) that leads to amplification of a pre-developed accretionary complex. The assumption for the oroclinal buckling (active II) is a slab break-off of the originally subducted slab as is illustrated in (b).

particular, the rheological behavior of the system can be influenced by perturbation of the thermal structure of the lithosphere associated with the elevation of lithospheric mantle, partial melting of the lower crust and the possible presence of felsic lower crustal material at the bottom of a continental domain (e.g. Maierová et al., 2018).

Convergent analogue models are characterized by ductile flow of the lower crust, regional folding and the formation of a range of brittle structures in the upper crust as a consequence of mechanical coupling between ductile and brittle layers (Brun, 2002). These processes are linked with the dynamic evolution of topography due to differential burial and uplift of the brittle upper crust related to vertical movements of deeper ductile crust forming the so-called pop-down structures (Cagnard et al., 2006). These topographical patterns are significantly more complex than those developed during lower crustal channel flow typical for continental collision tectonics (Beaumont et al., 2004, 2006; Duretz et al., 2011; Luján et al., 2010).

We examine the above mentioned complexities of boundary conditions and dynamically evolving interactions between the lower crust, mantle and upper brittle crust by means of analogue modelling in which we study the mechanism of oroclinal buckling by the folding of a vertical elastic beam confined by a horizontally stratified viscous medium. This approach is in contrast to existing analogue models where a buckled domain is represented by a single unit with free boundaries (Gutiérrez-Alonso et al., 2012; Pastor-Galán et al., 2012). Here we examine the shortening of a vertically layered lithospheric segment (e.g. Brun, 2002) immersed in low viscosity material without direct contact with immobile boundaries (Fig. 8, Fig. 9). In the set of experiments performed, we combine different horizontal stratification of silicon layers of variable viscosity for specific subdomains representing a relic of the oceanic lithosphere on one side and continental domain on the opposite side (Fig. 8, Fig. 9b). These subdomains are separated from each other by a steep subduction/accretionary complex. Such model geometry was set up to fit the geological evolution of the Central Asian Orogenic Belt (CAOB) – in particular the Mongolian oroclinal system (Yakubchuk, 2005). Its evolution is interpreted as a result of the oroclinal buckling of the subduction-accretionary belt after cessation of E-W subduction beneath the Mongolian continental ribbons followed by orthogonal, belt-parallel, N-S shortening of the whole zone in between the North China and Siberian cratonic jaws (Edel et al., 2014; Lehmann et al., 2010).

In this paper we focus on analogue experiments of oroclinal buckling of linear accretionary orogens developed after cessation of oceanic subduction, the formation of an accretionary wedge and Andean type thickening. During subsequent along-strike convergence, the accretionary system is deformed to produce a half-wavelength fold due to one-sided continental indentation or a full wavelength fold due to shortening of the system between continental jaws. The deformation of the domain is governed by the amplification of the orocline which has a sub-vertical axis and the formation of one or two hinge zones that indent the surrounding lithosphere. Lateral movement of fold hinges perpendicular to the shortening direction affects the surface structural patterns, regional topography and the complex 3D flow of the ductile crust and lithospheric mantle. The results of modeling are discussed on the basis of geophysically constrained crustal structure and surface deformation pattern of the Mongolian orocline.

2.2.1 Geodynamic setting of Mongolian orocline

The Kazakh and Mongolian oroclines are characterized by long lasting and orthogonal oceanic subduction beneath continental ribbons during the whole Early Paleozoic (Şengör et al., 1993). The architecture of this accretionary system (Fig. 8) is thus formed by a central continental ribbon and wide accretionary system similar to peri-Pacific accretionary systems in Japan or SE Asia. This belt was surrounded from one side by back-arc type oceanic lithosphere and from the other side by an accretionary wedge and subducting oceanic lithosphere from Cambrian to Silurian times (Fig. 8; e.g. Jiang et al., 2017; Wilhem et al., 2012). The evolution of the Mongolian orocline changed in the Devonian when the giant accretionary wedge

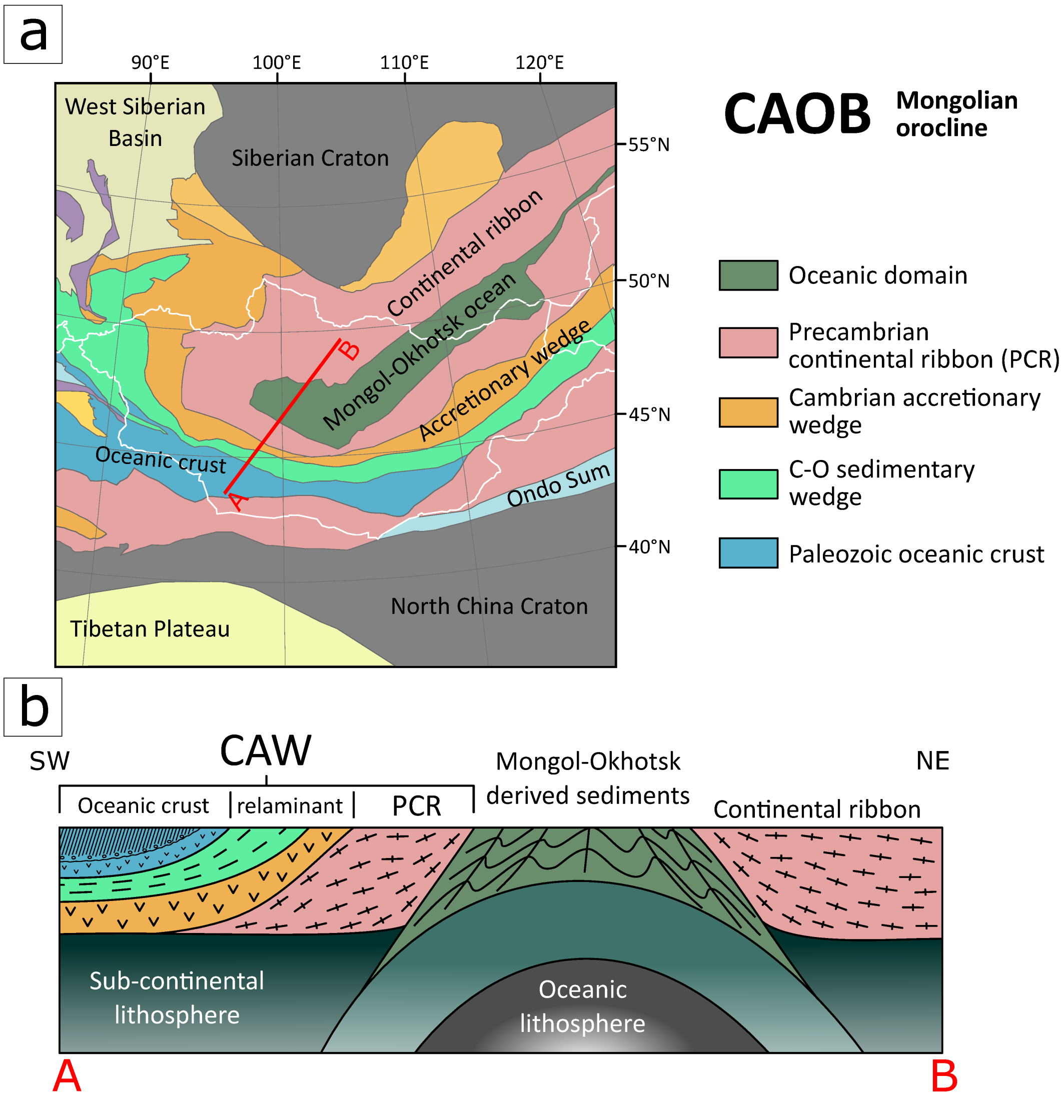

Fig. 8: Geological setting of the Tuva-Mongol orocline in the CAOB. (a) Geological background of modelled domain involving Mongol-Okhotsk oceanic domain, continental ribbon rimmed by the Cambrian accretionary, mainly volcanic, wedge, Cambro-Ordovician sedimentary wedge and Early Palaeozoic oceanic crust to the south. (b) The structure of the continental ribbon-accretionary wedge-hybrid lithosphere (CAW) represented by the relaminated, mostly felsic wedge, material beneath the oceanic crust (Guy et al., 2015; Nguyen et al., 2018) together with northerly continental ribbon. The oceanic domain is represented by the Mongol-Okhotsk oceanic lithosphere.

became molten above rolling back subduction. The wedge sediments were transformed to migmatites and granulites and flowed underneath the hanging wall oceanic plate generating vast gneissic relaminant (Guy et al., 2015). In that way originated a specific lithospheric structure marked by the existence of a continental ribbon, rimmed by an accretionary wedge partially transformed to high grade gneisses (Jiang et al., 2016) and by a hybrid lithosphere formed by an upper oceanic crust in addition to a lower crust formed by high grade gneisses issued from a metamorphosed accretionary wedge and possibly also a magmatic arc (Guy et al., 2015; Nguyen et al., 2018). This crustal segment can be considered as an embryonic and partly cratonized continental crust called here Continental Accretionary Wedge lithosphere (CAW). This specific setup was completed at the Carboniferous, when the whole complex system rotated together with Siberia in a clockwise manner (Cocks and Torsvik, 2007; Xiao et al., 2015; 2018). At the end of rotation, the Mongolian accretionary system was stitched to Siberia in the north, while its largest southern part pointed to the south. The belt was then surrounded by the Mongol Okhotsk Ocean in the east and a large subducting oceanic plate in the west (Fig. 8). It is also likely that the oroclinal bending of the subduction zone and CAW started to bend passively as illustrated by Lehmann et al. (2010) and Xiao et al. (2018).

The principal event modeled in this work is related to the Permo-Jurassic northward advance of the North China Craton (Edel et al., 2014) that resulted in the squeezing of the gently bended CAW between its northern edge and the southern boundary of northerly Siberia (Fig. 8). This stage resulted in massive shortening of the CAW which finally formed an isoclinal buckle fold surrounded by cratonic jaws. The core of the orocline was formed by the suture of the Mongol Okhotsk Ocean surrounded by the highly shortened CAW. The oroclinal buckling is accompanied by the formation of large scale E-W deformation zones similar to axial planar cleavage (Lehmann et al., 2010) and folding of horizontal strata between them. The deformation zones are characterized by narrow gravity anomalies implying important heterogeneous thickening of heavy upper oceanic crust (Guy et al., 2014). The hybrid lithosphere was transformed into a continental one i.e. into crust with intermediate granulitic lower crust, felsic middle crust and strong and brittle upper crust (Guy et al., 2015; Jiang et al., 2016; Nguyen et al., 2018).

It is important to understand how the whole laterally and vertically stratified system behaved during oroclinal buckling. In particular, the most interesting phenomena is the relative role of the buckled strong vertical layer, represented by a basement ribbon with a relic of subducted lithosphere, towards the advancing rigid North China Craton promontory, on vertical and horizontal fluxes of a weak relaminant and an underlying soft mantle. On the other hand, the complex lower crustal-mantle fluxes induced by buckling around a vertical axis and the surface deformation pattern related to upright folding with horizontal axis needs to be studied and understood. It is our plan here, to use analogue modeling and examine the above mentioned tectonic problems using a series of experiments which may lead to a better understanding of oroclinal bending processes which represents the most complex 3D tectonic system and may help to unravel the mechanical aspects of continental growth in general.

2.3 Model setup

In order to understand the 3D deformation of the complexly stratified CAW, we need to produce a model setup that will resemble the ancient peri-Pacific accretionary system described above before the beginning of oroclinal buckling. The setup thus represents the oceanic lithosphere, continental ribbon with relic of subducted lithosphere and hybrid domain marked by the presence of continental and viscous relaminant beneath the upper rigid oceanic crust.

2.3.1 Model geometry

Eight experiments were conducted to simulate oroclinal buckling of a linear, Pacific-type accretionary belt developed along a continental margin. Experiments were setup to simulate full-wavelength oroclinal buckling of the subduction zone with a vertical mechanical anisotropy, and oceanic (O) and continental (C = CAW) subdomains characterized by horizontal mechanical anisotropy. The modeled continental subdomain was isolated from the sandbox by silicone putty to minimize the negative effect of the boundary conditions represented by the immobile walls of the apparatus and to enable an investigation of material transfer during the shortening of the domain. The initial curvature of the accretionary subdomain controls the full wavelength buckling of vertically oriented anisotropy (Fig. 9a) and allows the complex 3D interactions between oceanic and continental subdomains to be modeled. All experiments were conducted in the same analogue modeling box (lateral, horizontal and vertical dimensions – 43 cm to 43 cm to 20 cm).

2.3.2 Model materials

In both experiments we simulated the large-scale oroclinal buckling process induced by the collision between two continental blocks. The work was inspired by models of Edel et al. (2014), Guy et al. (2014a) and Lehmann et al. (2010) concerning the development of the CAOB generated by the convergence of the North-China (the piston in our models) and the Siberia cratons (the rigid wall in our models).

All rock analogue materials have numerous limitations in mimicking real-world rock rheology. In some experiments it is suitable to use Newtonian silicone putties for approximation of viscous rheology (usually in the lower ductile lithospheric parts), while many advanced experiments (numerical and analogue sandboxes) use combinations of more complex rheologies (for details see Buiter and Schreurs, 2006). For example, the combination of a sand material for approximation of a brittle rheology in the upper lithospheric part - and in some four layer experiments in the

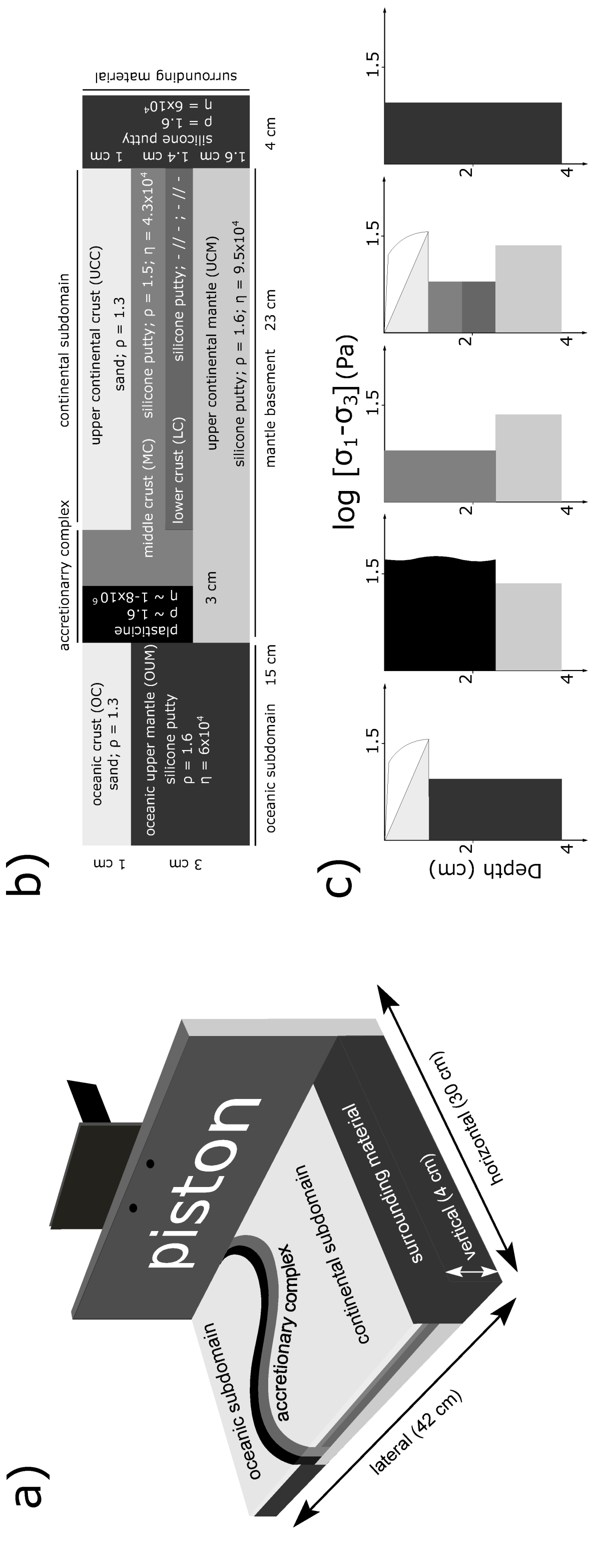

Fig. 9: Model setup of the oroclinal buckling experiments. 3D model view of the model domain with pre-folded orocline is shown in (a). The individual model layers with a specific material properties are illustrated in (b) with corresponding strength profiles in (c).

upper mantle segment (e.g. Brun, 2002) - with silicone putties (e.g. Cagnard et al., 2006) or with plasticine (e.g. Boutelier et al., 2008; Koyi and Mancktelow, 2001) for simulation of ductile flow of the lower crust and ductile mantle, is common. In other experiments, authors have used special types of plasticine for the construction of the whole model domain except for the upper crust or asthenosphere layer (e.g. in the modeling of oroclinal buckling, indentation, regional-scale folding, etc. (Duretz et al., 2011; Pastor-Galán et al., 2012; Tapponier et al., 1982)). Usually standard scaling methods based on the relationship between natural and laboratory conditions are used for the estimation of the model geometry aspects in combination with the applicability of a specific type of materials (e.g. Brun, 2002; Cobbold and Jackson, 1992; Davy and Cobbold, 1988; Davy and Cobbold, 1991; Hubbert, 1937; Ramberg, 1981).

In our experiments we used a combination of Fontainebleau sand (for modeling the brittle behavior of the upper crust – according to Byerlee, 1978), silicone putties (to represent a ductile crust and upper mantle segments) and plasticine (as a driving-layer of the buckling process i.e. an inner boundary condition). The rheological parameters of individual model layers are described in Tab. 1 and shown at Fig. 9b Fig. 9c. The horizontally layered continental subdomain is composed of silicone putty representing high viscosity upper mantle and low viscosity middle and lower crust, overlain by a Fontainebleau sand layer representing the brittle upper crust. This subdomain represents an oceanic upper crust relaminated by arc type lower crust and metasedimentary middle crustal layer of the CAW (Fig. 8). This subdomain is attached to a vertically layered accretionary subdomain composed of low viscosity silicone putty and a plasticine layer, underlain by silicone putty representing a high viscosity upper mantle. The plasticine layer drives the buckling process as displayed in Fig. 9a (for detail information regarding the use of plasticines for analogue models see Schöpfer and Zulauf (2002) or Pastor-Galán et al. (2012). In our experiments, this layer also represents an initial condition (i.e. a wavelength and amplitude are built into the layer prior to the deformation) that acts as an inner boundary condition. This step is not in conflict with model scaling because the aim of this study is to understand the flow of the lower crustal layers, the lithospheric mantle and the deformation of the upper crust associated with the buckling process. In all experiments the oceanic subdomain is composed of horizontal layers of silicone putty representing a high viscosity upper mantle and an oceanic crust overlain by a layer of Fontainebleau sand representing the brittle upper crust. This subdomain represents oceanic lithosphere of the Mongol-Okhotsk Ocean in Fig. 2. It should be noted that we reduced the friction between modeling box walls and the model materials by using petroleum jelly.

2.3.3 Model scaling

We followed the standard scaling techniques for the approximation of the geodynamic processes under laboratory conditions (see relations 1.1 - 1.6). Following

Tab. 1: Scaling model parameters.

		Upper crust	Middle - lower crust	Upper cont. mantle	Accretionary complex	Surrounding mat. / oc. mantle	Driving layer*
Density ρ (g . cm-^{3})	experiment	1.30	1.54	1.60	1.54	1.61	1.60
	nature	2.70	3.10	3.36	3.10	3.36	2.70
	scaling factor	0.481	0.497	0.480	0.497	0.482	0.59
Viscosity η (Pa . s)	experiment	-	4.30 x 10^{4}	9.50 x 10^{4}	4.30 x 10^{4}	6.50 x 10^{4}	-
	nature	-	1.13 x 10^{21}	5.00 x 10^{21}	1.13 x 10^{21}	5.00 x 10^{21}	-
	scaling factor	-	3.805 x 10^{-17}	1.90 x 10^{-17}	3.805 x 10^{-17}	1.20 x 10^{-17}	-
Material		Fontainebleau sand**	Silicone putty	Silicone putty	Silicone putty	Silicone putty	Plasticine

stable laboratory temperature: 18-21 °C
constant shortening rate

* two components (high viscosity silicone / thin-sheated plasticine)
** angle of internal friction ~30°

the examples of existing analogue experiments of indentation and shortening of lithospheric domains associated with faulting, surface elevation and displacement of the upper crust, the coupling and flow of lower crust, and the lithospheric mantle (e.g. Brun, 2002; Cagnard et al., 2006; Gapais et al., 2009), we set the model length to $30cm$, the model width to $42cm$ and model height to $4cm$ implying a space dimensions scaling factor $L^* = \frac{L_M}{L_N} = 8 \cdot 10^{-7}$. Due to the negligible role of gravitational Rayleigh-Taylor instability in our models, we ran all experiments under normal gravity acceleration implying $G^* = 1$. The scaling factor for densities ($P^* = \frac{\rho_M}{\rho_N}$) is in the range 0.481 and 0.497. For viscosity ($M^* = \frac{\eta_M}{\eta_N}$) the ratio varies from $1.2 \cdot 10^{-17}$ to $3.8 \cdot 10^{-17}$. From these scaling factors it is possible to obtain the factors for stress, time, strain-rate and velocity using the following relationships:

$$\sigma^* = P^* L^* G^*, \tag{2.1}$$

$$T^* = \frac{M^*}{\sigma^*} = t_M/t_N, \tag{2.2}$$

$$\varepsilon^* = \frac{\sigma^*}{M^*}, \tag{2.3}$$

$$V^* = \varepsilon^* \cdot L^*. \tag{2.4}$$

The Ramberg numbers for appropriate model parts are shown in Tab. 2.

2.3.4 Experimental procedure

In our experiments we applied finite strains represented by 25%, 37%, 45% and 50% horizontal shortening parallel to the lateral subdomain interfaces by the piston moving at a constant velocity of 2 cm/hour (Fig. 10). The laboratory temperature

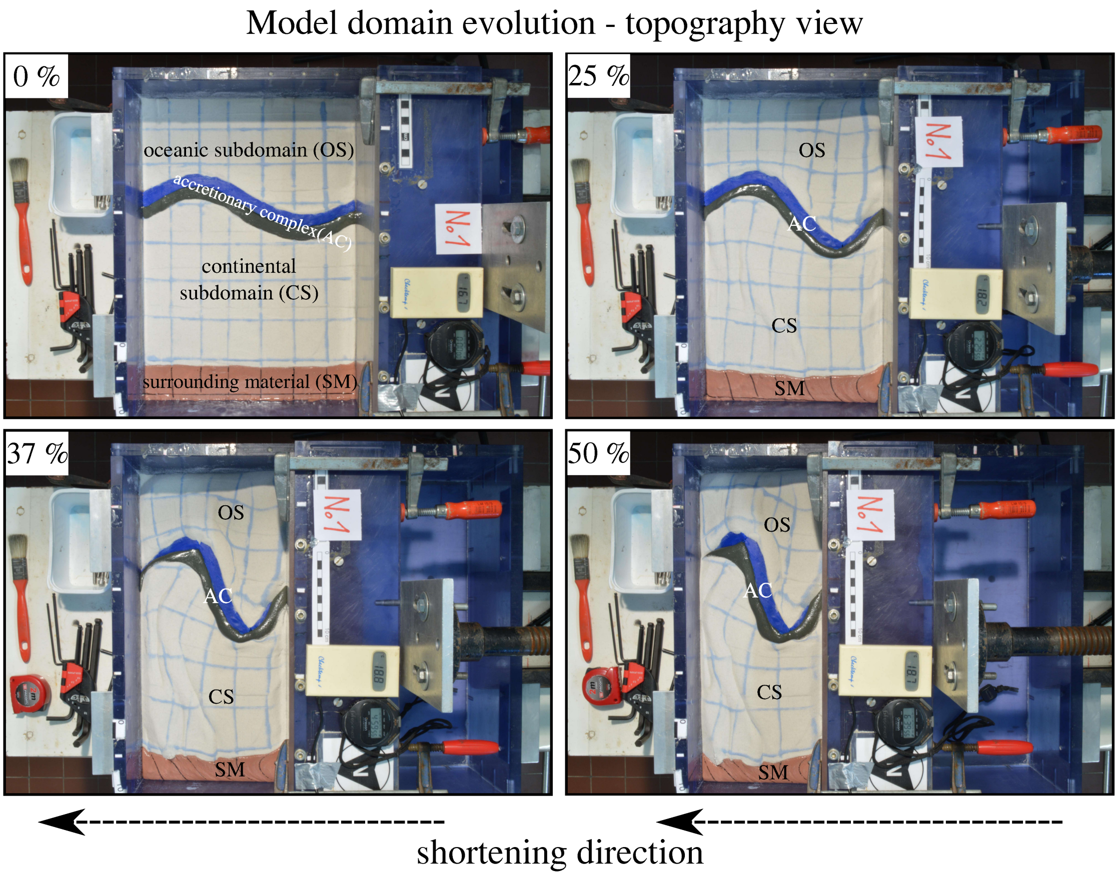

Fig. 10: Topographic view on experiment evolution after 0, 25, 37 and 50% of shortening.

during all experiments was 19 − 20 °C. To achieve different finite strain configurations, each type of experiment started from identical model setups (Fig. 9). All repeated experiments exhibited similar evolutions and verified reproducibility of the modelling. This comparison was performed according to the topography evolution and a visual inspection of model cross-sections. Only a few, negligible differences were noted and these were a result of small variations in the shape and thickness of the plasticine layer.

2.3.5 Model sectioning

An evaluation of the internal structures and mass redistributions was enabled by the sectioning of the deformed model domain along the major directions, i.e. normal to and parallel to the direction of shortening. To prepare these cross-sections, the model has to be frozen to eliminate undesirable deformation of silicon putty under its own weight. To obtain cross sections for different stages of model evolution, a series of identical experiments were carried out each being arrested after different amounts of shortening.

Tab. 2: Model scaling - Ramberg numbers

	model	original	scaling ratio
length (m)	0,03	30000	1,00E-06
time (s)	4500	3,15E+14	1,43E-11

Upper crust (sand in the experiment)	density ($kg \cdot m^{-3}$)	thickness (m)	inter. frict. coef.	coh. Strength (Pa)	Rs
model	1300	0,01	0,6	100	1
nature	2700	1,50E+04	0,6	5,00E+07	7

Lower crust (silicone in the experiment)	density ($kg \cdot m^{-3}$)	thickness (m)	viscosity (Pa·s)	grav.acc. (g) ($m \cdot s^{-2}$)	compr. rate V ($m \cdot s^{-1}$)	Rm
model	1540	0,014	4,30E+04	9,81	5,21E-06	13
nature	3100	1,50E+04	1,13E+21	9,81	6,34E-10	10

Upper continental mantle (silicone in the experiment)	density ($kg \cdot m^{-3}$)	thickness (m)*	viscosity (Pa·s)	grav.acc. (g) ($m \cdot s^{-2}$)	compr. rate V ($m \cdot s^{-1}$)	Rm
model	1600	0,01	4,30E+04	9,81	5,21E-06	7
nature	3360	1,50E+04	1,13E+21	9,81	6,34E-10	10

Upper oceanic mantle (silicone in the experiment)	density ($kg \cdot m^{-3}$)	thickness (m)*	viscosity (Pa·s)	grav.acc. (g) ($m \cdot s^{-2}$)	compr. rate V ($m \cdot s^{-1}$)	Rm
model	1610	0,024	6,50E+04	9,81	5,21E-06	27
nature	3360	3,50E+04	5,00E+21	9,81	6,34E-10	13

Accretionary complex (silicone in the experiment)	density ($kg \cdot m^{-3}$)	thickness (m)	viscosity (Pa·s)	grav.acc. (g) ($m \cdot s^{-2}$)	compr. rate V ($m \cdot s^{-1}$)	Rm
model	1540	0,024	4,30E+04	9,81	5,21E-06	39
nature	3100	3,50E+04	1,13E+21	9,81	6,34E-10	52

* thickness of the thin part of the upper mantle (nature) is proportional to model

2.3.6 Surface topography analysis

Four cameras with different elevations and view angles recorded model surface images every 10 or 5 minutes (determined by the final amount of finite shortening). One camera was situated directly above the experiment – for observing the evolution of the model surface from top view. This was used for 2D velocity fields reconstructions (PIV - particle image velocimetry). The other three cameras were used for the reconstruction of 3D model topography using the Micmac software (e.g. Galland et al., 2016).

For a detail investigation of upper crust deformation and topography evolution the PIVlab software was used (Thielicke and Stamhuis, 2014). This enabled displacement field characteristics, such as velocity magnitude, direction, horizontal components and divergence to be determined. The reconstruction of the velocity field provided an understanding of the model scale subsurface mass flow as well as the localized velocity gradients in specific parts of the model. The divergence of the velocity field was used to identify zones of localized thickening (negative divergence) or thinning (positive divergence) of the uppermost part of the model. These data were superimposed on the results obtained from the topography reconstruction obtained with the MicMac software to evaluate the mass transfer in a vertical direction.

2.4 Results

2.4.1 Finite geometry of modeled domain

In order to reconstruct lower crustal flow dynamics inside the modeled domain a set of perpendicularly oriented sections were analyzed. Both sections perpendicular and parallel to the shortening direction were obtained from two independent experiments with identical settings (Fig. 11 and Fig. 12).

2.4.2 Sections perpendicular to the shortening direction (i.e. parallel to the axial plane of the orocline)

The sections perpendicular to the shortening direction (referred as sections 1, 2, 3, 4 and 5 in Fig. 11) explore two contrasting domains; on the piston side of the model the fold hinge amplifies towards the continental subdomain (O→C, sections 1 and 2) and in the back stop part of the model the fold hinge amplifies towards the oceanic subdomain (C→O, sections 4 and 5). The inflection part of the fold is examined by section 3. These sections perpendicular to the shortening direction allow the investigation of horizontal and vertical material flows perpendicular to the direction of shortening in the oceanic subdomain (section 1), across the accretionary subdomain area (sections 2, 3, 4) and in the continental subdomain (section 5). Sections 1 and 2 (O→C) show similar pattern characterized by generalized thickening of the ductile part of oceanic and continental lithosphere. The main feature is the shortening of the continental subdomain parallel to the piston boundary resulting in underthrusting of the continental subdomain below the oceanic one. This movement is accompanied by exhumation of the subcontinental mantle beneath the propagating fold hinge and upright folding of the continental crust-mantle interface. Section 3 (across the fold inflection) shows horizontal movements limited to the sub-continental and oceanic mantle lithosphere which is accompanied with minor extrusion of continental mantle beneath the accretionary subdomain. The two sections 4 and 5 (C→O) show considerably thinner ductile part of continental subdomain compared to the O→C sections. This is accompanied with flow of sub-continental mantle lithosphere over the oceanic one in the fold hinge zone.

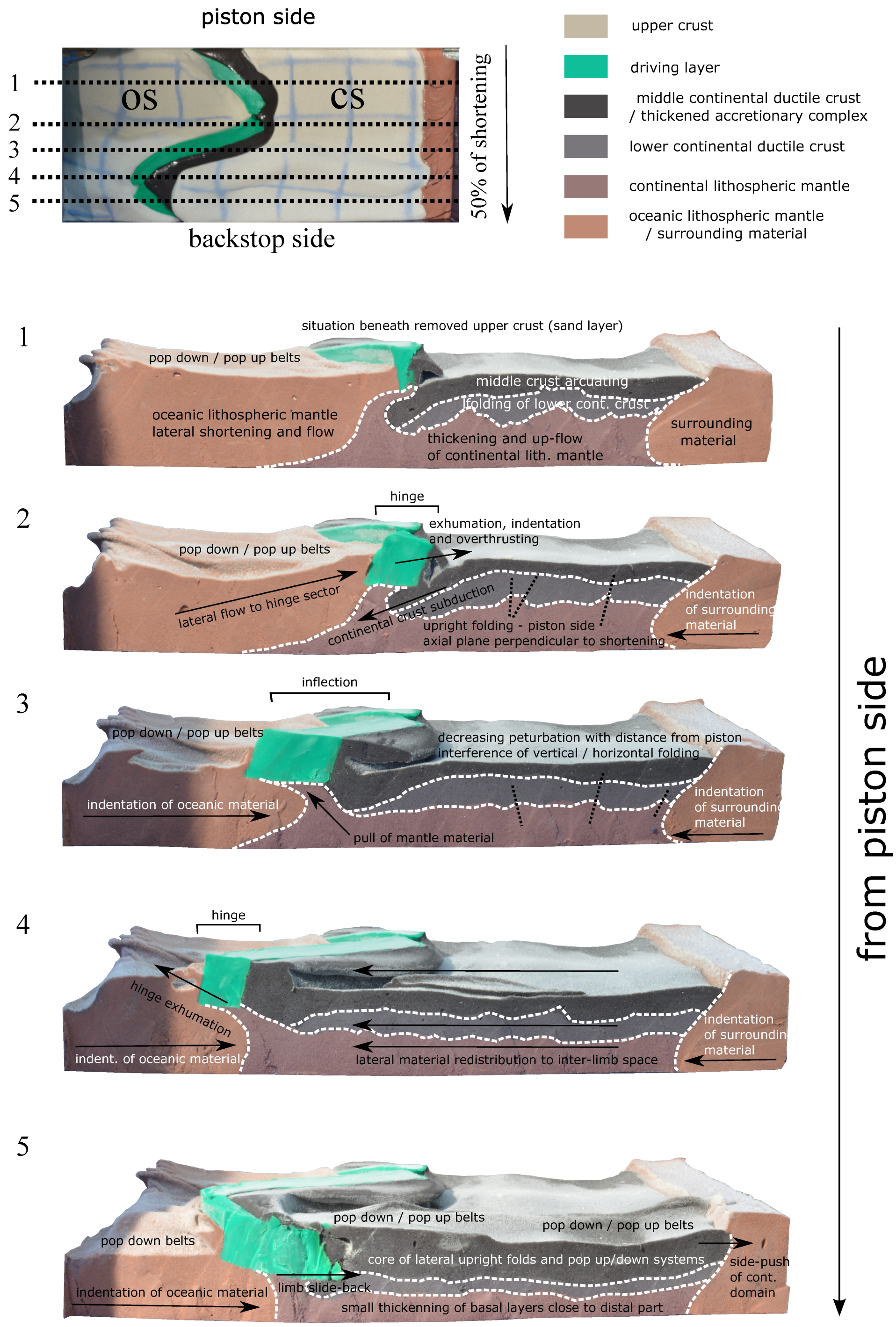

Fig. 11: The sections perpendicular to shortening. The orientation map of individual cross-sections of sliced domain is situated on top of the figure. The cross-sections display major structures and sense of material movement (arrows direction) in different parts of whole domain.

2.4.3 Sections parallel to the shortening direction (i.e. perpendicular to the orocline axial plane)

The sections parallel to the shortening direction (referred to as sections 1, 2, 3, 4, 5 and 6 in Fig. 12) explore the contrasting evolution of oceanic and continental subdomains. The oceanic subdomain (section 1) reveals significant and heterogeneous thickening of the oceanic lithosphere, which is most pronounced close to the piston boundary. This section intercepts the tip of the C→O fold hinge which has been exhumed. Subcontinental mantle has flowed laterally and this now occupies the region beneath the fold hinge. The shortening is accompanied by the deformation of the mantle-crust interface which now exhibits pop-down structures similar to those described by Cagnard et al. (2006). In contrast, the continental subdomain (sections 5 and 6) typically shows pronounced thickening of mantle lithosphere towards the piston accompanied by thickening of ductile crust and thinning of the mantle towards the back stop. The crustal deformation is localized in the axial plane of the hinge area of the C→O fold hinge and is manifested by the formation of pop down structures and cuspate-lobate folding of the crust-mantle interface. Section 4 intercepts the tip of the O→C fold hinge and exhibits overall homogeneous shortening of the whole lithosphere. This is expressed by pop-down structures along the upper-middle crust boundary and by cuspate-lobate upright folding of both the crust-mantle and lower-middle crust interfaces. Section 3 is typified by a contrasting response of the continental and oceanic subdomains. The continental subdomain fold hinge forms an antiformal domal structure formed by middle crust surrounded with marginal synforms and cored by lower crust and mantle associated with cuspate-lobate folding of the crust-mantle interface. The oceanic crust-mantle boundary is characterized by the formation of pop-down structures while the interface between oceanic and continental mantle forms large scale synformal structure. The main feature of section 2 is the influx of the oceanic mantle into the continental subdomain below the amplified crustal antiformal domal structure.

2.4.4 Incremental evolution

The two previous paragraphs described spatial variations in finite deformation pattern corresponding to a bulk shortening of 50%. Here, we make an attempt to understand the evolution of these structures by means of analysis of the incremental deformations. This is achieved by examination of sections across the continental and accretionary subdomains for three repeated identical experiments with different finite shortening 25%, 37% and 45% (Fig. 13). The folded accretionary subdomain (sections A-B) reveals contrasting behavior of the oceanic and continental subdomains. The early shortening (25%) is accommodated mainly by thickening of the oceanic lithosphere. In the second stage (37% shortening) a massive flux of oceanic mantle from the O→C hinge area towards the continental subdomain, can be observed. This flow causes the formation of an antiformal structure with a sub-horizontal

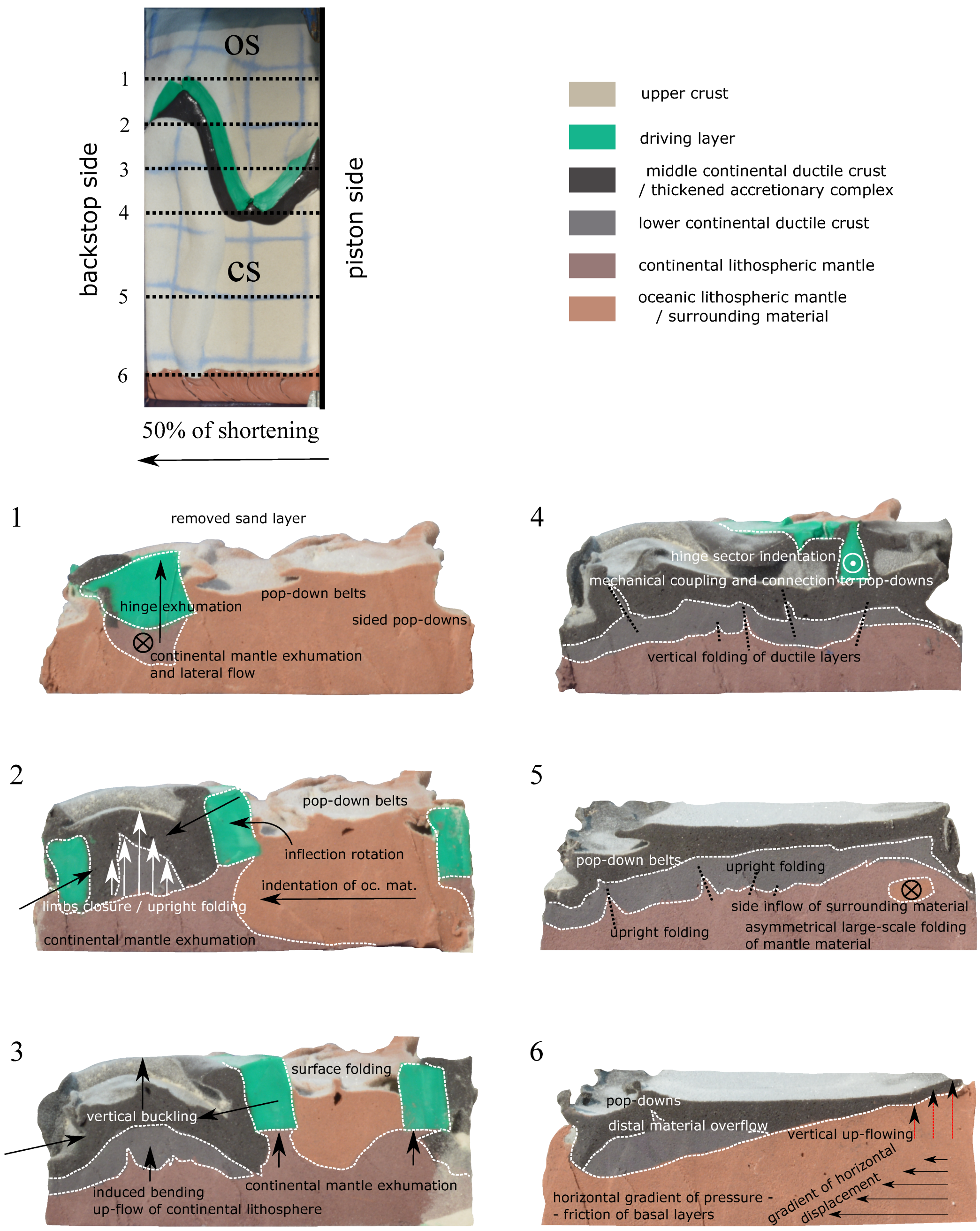

Fig. 12: The sections parallel to shortening. The orientation map of individual sections of sliced domain is situated on a top of figure. The cross-sections display major structures and sense of material movement (arrows direction) in different parts of whole domain.

fold axis in the region of the axial plane of the C→O fold (which has a steeply plunging fold axis. The subsequent stage of deformation (45% shortening) shows an amplification of the antiformal dome structure cored by continental lower crust that has been massively shortened by oceanic mantle lithosphere indentation. Here, the crustal antiformal dome is decoupled from continental mantle due to under thrusting of oceanic lithosphere. The evolution described above is accompanied by the dynamic deformation of the upper crust which is progressively uplifted in the C→O fold domain while in the O→C hinge area forms a synform which evolves into a large-scale pop down structure with ongoing shortening (45%).

The continental subdomain (sections C-D Fig. 13) reveals contrasting behavior of the crust and the lithospheric mantle during progressive shortening. The lithospheric mantle exhibits a classical indentation profile marked by an increase in thickening towards the piston (England and Houseman, 1986). As a consequence, a giant mantle dome structure develops close to the piston with attenuated crust in the apical part of the dome. In contrast, both the upper and lower continental crust thicken as they are traced away from the piston. While the upper crust is thickened as a result of thrusting and buckle folding, the middle and lower crust thickening occurs by homogeneous shortening associated with the development of cuspate-lobate structures at the mantle-lower crust, and lower-middle crust interfaces. Cuspate-lobate instabilities typically develop at boundaries between low viscosity contrast materials, when subjected to layer-parallel compression.

2.4.5 Evolution of model surface deformation

The analysis of the surface (Fig. 14) reflects the deformation of upper crust represented by the sand layer, which is removed before model sectioning. PIV analysis was used to assess the deformation of the uppermost crust during shortening. The deformation of the model surface was analyzed by inspection of the shear strain and velocity field (Fig. 14a) patterns for four shortening stages (3%, 25%, 37% and 45%) and the corresponding divergence of the velocity field (Fig. 14b). The deformation of the surface and corresponding response at depth are shown in a series of interpretative cross-sections for several model runs (Fig. 14c). For detailed analysis of the surface deformation, we refer the reader to follow the technical article aimed to application of the PIV technique for strain-analysis of indentation experiments including oroclinal buckling models (Krýza et al., 2019).

The beginning of the experiment (3% shortening) develops a homogeneous deformation in the continental subdomain (Fig. 14a) which is perturbed in the vicinity of the accretionary domain by the initiation of an active buckling (Fig. 14b). This could be detected by variations in the orientation of the velocity vectors which were observed up to a bulk shortening of 25% followed by a velocity field typical of post-buckle flattening (i.e. parallel velocity vectors). For subsequent increments of shortening (25% and 37%) the surface deformation partitioning can

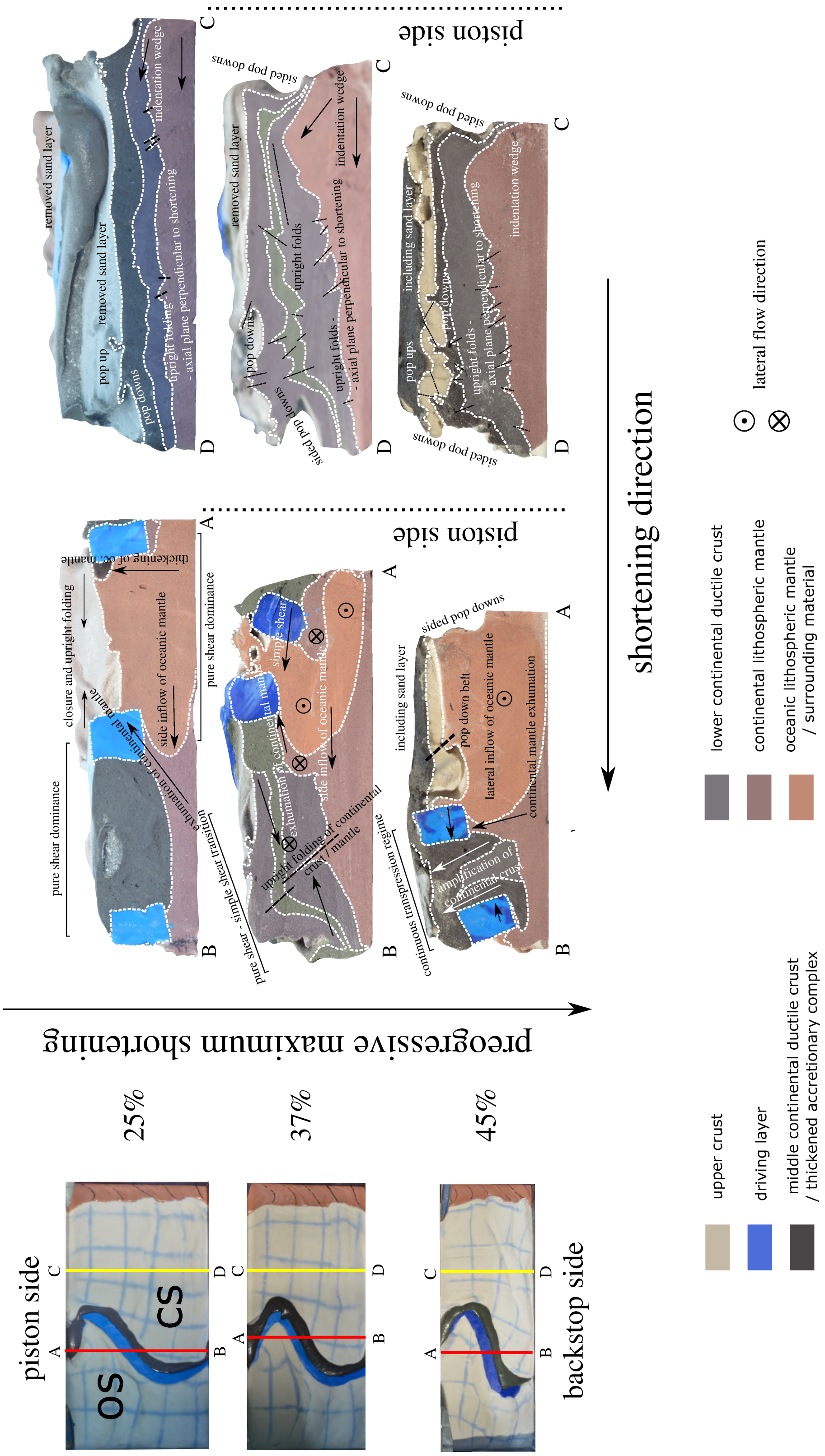

Fig. 13: The incremental evolution of the model domain. Three different stages of the shortening are shown at the left side with two lines for sectioning (red/yellow). The corresponding cross-sections at the right reveal the progressive development of a major deformation features inside the model domain.

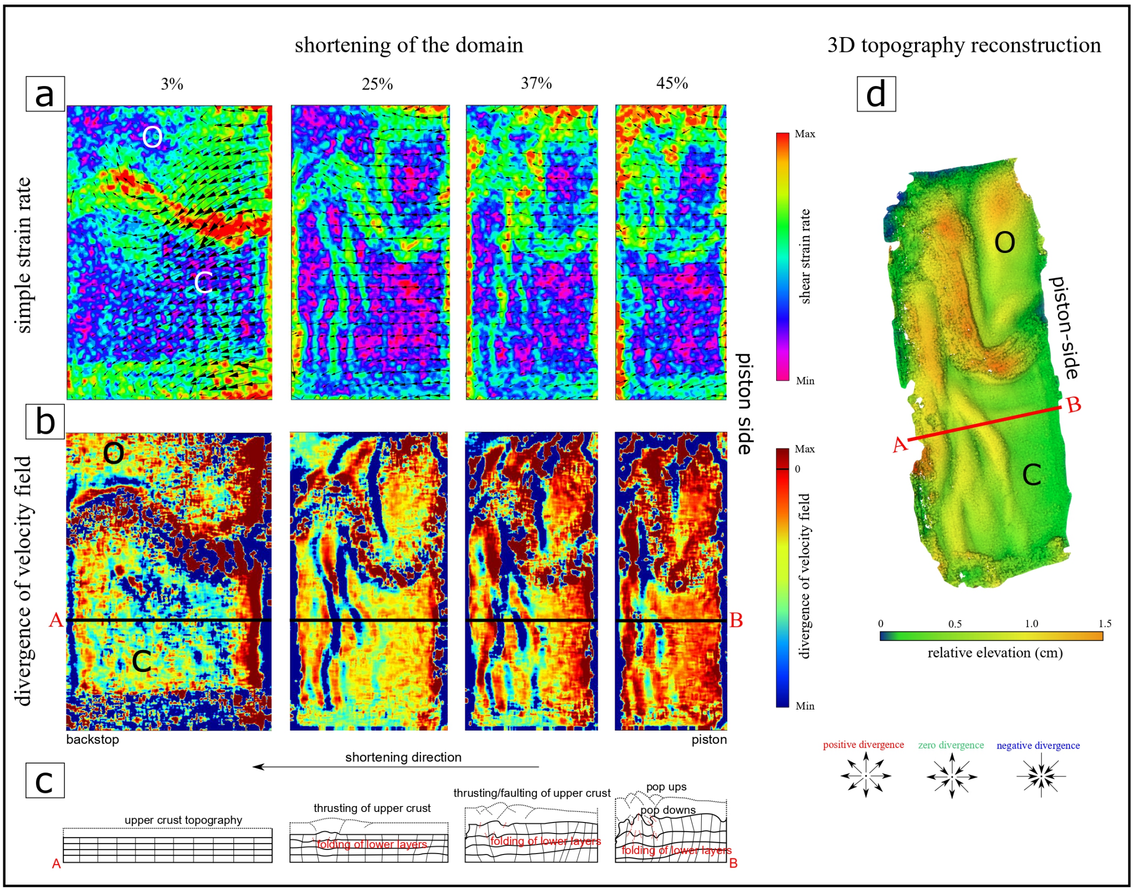

Fig. 14: The model surface analysis. For reconstruction of material transfer at the surface we analyzed the displacement field calculated by PIVlab software. Panel (a) represents a shear strain rate where arrows correspond to the velocity field. The divergence of the velocity field is shown in panel (b) where major anomalies in the field are related to the development of pop ups and synclines (c). The finite topography map is shown in (d). The digital elevation model (DEM) in panel (d) is modified after Krýza et al. (2019).

be observed in both the oceanic and continental subdomains where narrow zones of deformation gradients are developed parallel to fold axial planes (Fig. 14b – blue zones). With ongoing deformation (45% shortening) the domains separate into two areas characterized by different shear strain rate (contours on Fig. 14a); high strain rates in the oceanic domain and low strain rates in the continental domain.

This evolution can be clearly seen in the field of the velocity divergence (Fig. 14b). This shows a noisy pattern for small shortening (3%) reflecting homogeneous deformation. With the development of narrow zones of localized deformation (folding) the velocity field becomes characterized by high frequency negative and positive anomalies which developed preferentially along the axial plane of the C→O fold hinge in the continental subdomain and along the axial plane of the O→C fold in the oceanic domain. These anomalies correspond to the development of thrust related folds which are initial of the pop-up structures (e.g. Brun, 2002) and the narrow synclines associated with the development of pop-down structures at deeper crustal levels described above (Fig. 14c).

The final topography reconstruction after 50% shortening (Fig. 14d) shows well developed positive topography anomalies along the folded accretionary subdomain and positive narrow linear ranges correspond to thrust related folds. The narrow and low topography anomalies alternate with the above mentioned negative values of divergence and correspond to narrow synclines, while large topography anomalies correspond to positive values of divergence that are associated with the development of the pop-up structures. The wide plateaus of neutral to high topography are developed in both oceanic and continental subdomains close to the piston side.

2.5 Discussion

2.5.1 Model limitations

As with most physical models our experiments are limited by the presence of un-geological boundary conditions which are represented by the fixed walls of the model box. The presence of these boundaries affect the model behavior adjacent to the walls. This can be clearly seen for example on the contour maps of dynamic parameters provided by the PIV calculations and it is possible to distinguish pop-down structures that form as a result of these boundary conditions and which do not relate to structures that might form in nature. However, we argue that the deformation in the inner regions of the model is unaffected by the size of model box and its fixed walls. The planar indentation profile (e.g. England and Houseman, 1986; Tapponier et al., 1982) will be developed in the inner domain of model independently of the box size and model results will not be affected.

The model setup represents an identical geometry to the model domain for all experiments that we analyzed. The subject of this article is not to prepare a parametric study but to bring new insights to mass transfer associated with oroclinal buckling on a lithospheric scale. In future models, we plan to test the effect of different convergent scenarios (e.g. various angle of convergence, shortening rate), and to incorporate an asthenospheric mantle or thermal aspect to the modelling. In the present model we have neglected any initial, pre-buckle, thickening of the model domain and supported orocline amplification by the pre-folding of the accretionary belt (See 0% shortening in Fig. 10). The geometry of pre-folded layers (O→C in the indenter side, C→O in the back-stop side) has been chosen in order to simulate material flow in a specific geological example namely the Mongol orocline after the subduction of the Mongol-Okhotsk oceanic domain (e.g. Lehmann et al., 2010; Edel et al., 2014). This scenario represents only the first part of the model domain (O→C) up to inflection of orocline.

2.5.2 Rheological interfaces and associated model dynamics

The model for oroclinal buckling is composed by a several silicone and sand layers according to the model setup. All interfaces between these layers i.e. inner boundaries represent transitions between domains of various rheological and/or mechanical properties. Here we discuss how general flow and deformation of the model domain is affected by these zones of heterogeneities. In the whole domain, it is possible to distinguish three types of rheological interfaces between the sand (brittle), silicone putty (viscous) and plasticine (plastic) materials: 1. brittle/viscous interface between the upper crust and middle/lower crust in the continental subdomain and between the crust and mantle in the oceanic subdomain; 2. plastic/viscous interfaces between the folded accretionary wedge (vertical subdomain) and both crust and mantle of oceanic and continental subdomains and 3. plastic/brittle interface is only present as the lateral boundary between folded accretionary wedge and oceanic upper crust. In addition, there are transitions between viscous materials of different viscosities reflecting lower crust-mantle transition within the continental and oceanic subdomains. Here we discuss the mechanical role of those interfaces in terms of mechanical coupling and/or decoupling during model evolution.

The major zone of mechanical decoupling is developed along the interface between the brittle upper crust (sand) and viscous middle-lower crust (silicone putty) generally called brittle-ductile transition. It is manifested by contrasting deformation patterns developed within viscous and brittle parts until 40% of shortening. While the viscous part of the model exhibits typical indentation profile in front of the piston, the brittle layer is detached and most of the deformation is localized along the axial plane of C→O fold. During subsequent shortening, this behavior progressively vanishes and both parts of the model exhibit more coupled deformation.

We can distinguish two types of brittle parts of the model according to the types of surrounding interfaces. While brittle part of continental subdomains is exclusively surrounded by viscous materials (except free-slip boundaries with piston and backstop of the model box), the brittle part of oceanic subdomains has different lateral interfaces with both plasticine and model box boundary. Such a configuration is manifested by the contrasting distribution of deformation (Fig. 10 and Fig. 14a,b) during initial shortening (up to 25%). We suggest that this behavior also affects the contrasting distribution of finite deformation within the upper crust of oceanic subdomain in respect to the continental subdomain.

Both plastic/viscous interface and transitions between viscous materials of different viscosities exhibit strong mechanical coupling during experiments and any significant differential motions have not been observed.

2.5.3 Mantle and crustal fluxes related to oroclinal buckling

The analyses of finite strain patterns along the axial plane of an orocline and on sections parallel and orthogonal to the shortening direction together with a study of the incremental evolutions of these sections and surfaces, allow the relationships between deep lithospheric fluxes and surface deformation related to oroclinal buckling to be determined. At the level of the lithospheric mantle, we observe classical indentation profiles in both oceanic and continental subdomains characterized by progressive thickening towards the piston boundary. However, below the folded accretionary domain the deformation pattern is different. Here, the lateral fluxes parallel to the fold axial planes dominate the deformation of both types of mantle lithosphere which are dragged by migrating fold hinges in a vortex manner. In this way the two contrasting mantle lithospheres are laterally juxtaposed where oceanic mantle flows towards the hinge domain of the O→C fold and continental lithosphere flows towards the C→O fold. The less competent oceanic mantle flows more efficiently to the O→C fold hinge area compared to slowly flowing subcontinental mantle. The lack of balance in mantle fluxes has a profound effect on the continental deformation which reacts by efficient flux of continental crust into the C→O fold hinge. These redistributions of mantle and crustal materials are associated with the formation of antiformal fold with horizontal axis in the region of the C→O fold and horizontal synform in the O→C fold domain. These processes are also reflected in the surface where pop-down structures dominate the O→C hinge while the C→O hinge shows the presence of a central antiform surrounded by narrow, marginal synclines (Fig. 15).

The consequence of unbalanced mantle fluxes leads to the development of a region dominated by crustal material in the C→O hinge compared to mantle dominated region in the O→C hinge zones. Mechanically, the C→O hinge is represented by a multilayer system formed by stiff continental mantle at the bottom, overlain by extremely weak lower crustal layer and strong middle and upper crust higher in the column. In contrast, the O→C hinge is formed exclusively by weak oceanic mantle and thin upper crust. Therefore, the integrated strength of the C→O multilayer system (England and Houseman, 1986; England and Houseman, 1989; Thompson et al., 2001) is significantly lower compared to adjacent O→C lithosphere. This difference implies that under horizontal compression the C→O system collapses and shortens preferentially. The deformation is controlled by the presence of a strong substratum overlain by a weak layer which is an ideal condition for detachment of a weak lower crust from the rigid upper mantle and the buckling of the stronger, middle-upper crustal layer. The formation of the detachment antiform in the C→O domain is accompanied by flux of oceanic mantle and the progressive development of material deficit in the OC region close to piston leading to the formation of large scale synform filled by oceanic crust decorated by pop-down structures at the surface.